Flexural Properties of UHPFRC Beams with an Initial Notch

Younes Baghaei Osgouei[1], Shahriar Tavousi Tafreshi[1*], Masoud Pourbaba[3]

1. Ph.D. Candidate, Department of Civil Engineering, Faculty of Civil and Earth Resources Engineering, Central Tehran Branch, Islamic Azad University, Tehran, Iran
2. Assistant Professor, Department of Civil Engineering, Faculty of Civil and Earth Resources Engineering, Central Tehran Branch, Islamic Azad University, Tehran, Iran
3. Assistant Professor, Department of Civil Engineering, Maragheh Branch, Islamic Azad University, Maragheh, Iran

Corresponding author: *sh_tavousi@iauctb.ac.ir*

ARTICLE INFO

ABSTRACT

Experimental and numerical studies are carried out in this study to characterize the flexural properties of ultra-high-performance fiber-reinforced concrete (UHPFRC) beams with and without an initial notch reinforced with micro steel fibers in overall ratios of 2% by volume. Dimensions of the notch were 5 mm in width, and 25 mm in height. For this purpose, three-point bending tests were carried out on UHPFRC specimens. Thereafter, numerical studies were carried out to validate experimental findings and in subsequent, sensitivity analyses were carried out to provide better insight with regard to the investigated parameters. Variables of the study were: mesh size, width, height, length, overall size of the beam, tensile strength, compressive strength, modulus of elasticity, crack mouth-opening displacement (CMOD), and crack tip-opening displacement (CTOD). Furthermore, vertical deflection-CMOD findings were compared against available equations in the literature and discussions were made where relevant. Results showed that finer mesh leads to negligible stiffer results with similar observations for the maximum sustained stress by the modulus of elasticity, compressive strength, and width variations. Moreover, 40% increase in the tensile strength led to 47% increase in the sustained stress and doubling the clear span led to 5.5% increase in the sustained stress and 20% peak deflection.; depth variations led to size effect phenomenon and nonlinear regression analyses successfully captured the flexural load-deflection, load-CMOD, and load-CTOD trends of the flexural beams with coefficient of correlation values (R^2) close to unity. Finally, a brief cost analysis was given for the fabrication of 1 m^3 of UHPFRC.

1. Introduction

Emergence of a new class of cementitious material namely, ultra-high-performance concrete (UHPC), has been a turning point in the technology of concrete. This material in combination with various types of steel, synthetic, natural, and mineral fibers, which address and/or improve shortcomings of this material, among which the most important one is the tensile strength. Ultra-high-performance fiber-reinforced concrete (UHPFRC) has shown excellent mechanical and durability properties as reported by several researchers [1], to name but a few. Nonetheless, compared to the conventional concrete, performance of UHPFRC, as a promising material for resilient structures, is relatively unknown under various loading conditions. For instance, there is not a consensus on the definition of its compressive strength; Association Francaise deG´enie Civi (AFGC) [2], and ACI-239 [3] define UHPFRC as a material with $f_c' \geq 150$ MPa, where f_c' is the compressive strength of concrete. According to Fédération Internationale du Béton (FIB) [4] this value is 120 MPa, whereas EN 206 [5] considers 100 MPa as the threshold. In line with the need to address essential features of UHPFRC required for practical applications and numerical simulations, the objective of this study is to characterize the behavior of notched UHPFRC beams under three-point-bending (3PBT) through experimental and numerical analyses and make comparisons with the existing literature where relevant.

Over the last two decades, a new class of cementitious composites has been developed with the reactive powder concrete (RPC) by Richard and Cheyrezy [6] being the fore-runner. This new cementitious composite, namely ultra-high-performance concrete (UHPC) is characterized by low water-to-cement (W/C) ratio, high-range water-reducing agent (HRWRA), silica fume, quartz powder, and fine sand. According to numerous studies available in the literature, this material outperforms the conventional normal-strength concrete (NSC) both on the material and structural level with its main drawback being its brittleness. With regard to the foregoing, the issue is resolved by the incorporation of various type of fibers, each with its respective application (see Table 1). Ultra-high-performance fiber-reinforced concrete (UHPFRC) is good for rehabilitation purposes [8], flexural [9], tensile [10], and shear [11].

Additionally, the high compressive strength of UHPFRC results in a remarkable reduction in the weight of structures made from this material. Generally, the overall weight of structures made from UHPFRC is only one-third to one-half the weight of typical reinforced concrete (RC) structures under the same load [12]. Superior attributes that fibers add to a cementitious composite are highlighted in Tables 2 and 3, among which elongation is the most important one as it addresses the brittleness of normal concrete in tension.

Table 1. Performance of different fibers [7].

Fiber type	Composite Performance		Economic and Environmental Impact		Comments
	Tensile Ductility	Crack width (μm)	Cost	Embodied energy	
Aramid	Moderate	10-30	High	High	Structural, low ductility
Basalt	Low	-	Low	Low	Structural, low ductility
Carbon	Low	-	High	High	Structural, low ductility. Self-sensing
Glass	Low	-	Low	Low	Structural, low ductility
Nylon	High	>100	Comparable to PVA	High	Structural, high ductility
PBO	Moderate	10-30	High	High	Structural, low ductility. high strength
PE	High	50-150	High	Comparable to PVA	Structural, high ductility. High strength
PET	Moderate	150-200	Low	Low	Non-structural
PP	High	70-260	Low	Comparable to PVA	Structural, high ductility. low strength
PVA	High	<100	-	-	General structural applications
Steel	Moderate	10-30	High	High	Structural, low ductility. High strength

Note: Ductility is with reference to that of ECC, i.e. low (<1%), moderate (1-2%), and high (>2%). Cost and embodied energy are with reference to that of PVA

Table 2. Technical specifications of different fibers [7].

Fiber type	Diameter (μm)	Length (mm)	Density (g/cm^3)	Young's Modulus (GPa)	Elongation (%)	Melting/decomposition temperature (℃)
PVA	39	8-12	1600	42.8	6	230
PBO[*]	13	6	5800	180-270	2.5-3.5	650
Carbon	6.8-20	3-18	525-4660	33-268	0.8-2.4	1150-1200
Steel	150-1000	13-25	350-2000	210	2-4	>1425
PE	24-38	12	1950-3000	39-100	3.1-8.0	150
Basalt	15-16	12	2230-4840	85.8-89.0	2.85-3.15	>1400
Glass	6-20	3-6	2000-4000	70-80	2.0-3.5	>1400
Aramid	12	6	3400	74	4.5	500
PET	38	12	1095	10.7	22	255
PP	12-41	6-12	850-928	2.7-9.0	7.3-30	160
Nylon	8	19	966	6	18	220

 * PBO: Poly (p-phenylene-2, 6-benzobisoxazole)

Table 3. Advantages and disadvantages of UHPC [13].

Advantages	Disadvantages
✓ High compressive strength- rapid strength gain	
✓ Higher tensile strength before and after cracking in comparison to normal concrete	✕ Relatively high cost
✓ Very high ductility in comparison to normal concrete	✕ Susceptible to high autogenous shrinkage given its low water: binder ratio
✓ Excellent durability properties- innocuous to alkali-silica reaction	✕ Rigorous necessity for curing environment if early stage and lower later stage shrinkage are needed
✓ Exceptional toughness indices	
✓ Lower shrinkage and creep after steam treatment	

Given the superior characteristics of UHPC to NSC, this cementitious composite is increasingly being used in different civil engineering sectors such as bridge engineering, slender structures, hybrid structures, etc. However, high cost of its constituents and sometimes special preparatory requirements have limited the use of UHPC worldwide [13].

Fibers can be categorized into two categories, man-made and natural fibers which are sub-divided into two and three categories as follows:

Man-made fibers: (1) inorganic: Basalt-Carbon- Glass- Steel, and (2) Polymeric: Nylon- Polyethylene (PE)- Polypropylene (PP)- Polyvinyl alcohol (PVA)

Natural fibers: (1) Plant: Coir- Sisal-etc., (2) Animal: Silk- Wool, and (3) Mineral: Asbestos- Wollastonite.

Discontinuous steel fibers are the most-widely one. The main purpose of adding steel fibers is to enhance both ductility and toughness. A summary of different steel fibers is given in Table 4. Straight steel fibers have higher contact angles which make the fibers hydrophobic and hence, resulting in weaker interfacial/matrix bond. For this reason, steel fibers with various geometries are used to counter this disadvantage.

Conflicting studies exist in the literature which on one hand emphasize on the better performance of smooth micro steel (MS) fibers while others have concluded that deformed steel fibers outperform MS fibers almost in all the mechanical properties [7]. Higher aspect ratios and volumetric contents contribute to the improvement of the mechanical properties except for the compressive strength, regarding which, minimal increase of compressive strength has been reported.

Man-made fibers are mainly supplied in masses while its common to express the performance of fiber-incorporated cementitious composites in volumetric ratios. Hence, besides Fig. 1(a), Fig. 1(b) has been presented. Steel, PET, glass, basalt, and acrylic fibers are cheaper than PVA among which steel, and glass fibers offer satisfactory mechanical performance according to the available literature. On a volumetric basis, nonetheless, steel, and basalt fibers offer higher densities and therefore are less favorable.

CO_2 footprint is a deleterious outcome of the fiber production. Mostly, fibers with higher energy intensity give out higher CO_2 content as suggested in Table 5. The CO_2 content of steel fibers is less than its PVA counterpart on the mass scale but is well higher than it if measured on a volume basis.

Concerning the embodied energy, according to Table 6, glass and basalt fibers demonstrate the lowest energy regardless of being measured on a mass or volumetric basis. For steel fibers, mass scale shows low energy intensity but the converse is true for the volume scale.
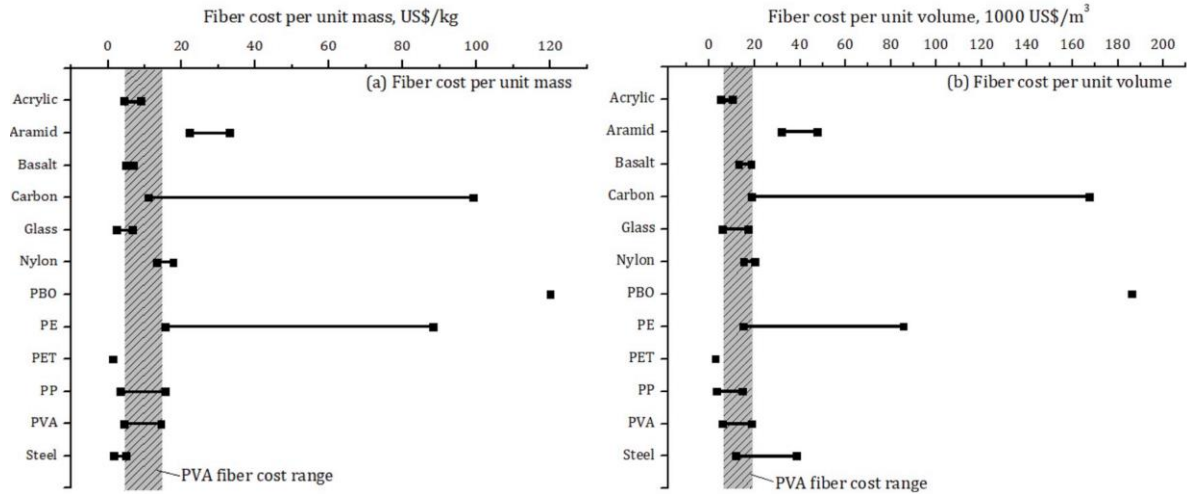
Fig. 1. Range of fiber cost (a) by mass (b) by volume [9].

Table 4. Properties and performance of steel fibers incorporated in cementitious composites.

Ref.	Geometrical Parameters			Volume (%)	Tensile Performance	
	Length (mm)	Diameter (μm)	Shape		Strength (MPa)	Strain Capacity (%)
Li et al. [14]	6-20	150	Straight	2.3	8	0.49
Wille et al. [15]	13-30	200, 300, 380	Twisted-Hooked	2.5	12.4	0.49
Naaman [16]	30	300	Twisted	2	13.6	1.25
Maalej and Li [17]	6	150	Straight	1	4	Quasi-brittle
Joo-Kim et al. [18]	30	300, 380	Twisted-Hooked	2	8.7	0.52
Tran and Kim [19]	30	300, 375	Twisted-Hooked	1	6	0.50
Kanakubo [20]	15	200	Straight	2	12.4	0.09
Naaman and Homrich [21]	30	500	Deformed-Hooked	12	28	1.00-2.00

Table 5. CO2 content embodied in different fibers.

Fiber	CO_2 emissions per unit mass (**kg/kg**)	CO_2 emissions per unit volume	Ref.
Acrylic	33.50	39.50	Hassan et al. [22]
Aramid	-	-	-
Basalt	-	-	-
Carbon	29.40	49.60	ELG Carbon Fiber Ltd. [23]
Glass	0.16	0.42	Dai et al. [24]
Nylon	-	-	-
PBO	-	-	-
PE[a]	2.00	1.90	Greene [25]
PET[b]	0.81-3.40	1.10-4.60	Yu et al. [26]
PP	2.00	1.87	Greene [25]
PVA	1.71	2.22	Keoleian et al. [27]
Steel	1.61	12.5	Kim et al. [28]

[a] : Low-density PE.

[b] : Virgin PET.

Table 6. Intensity of embodied energy for different fibers.

Fiber	Energy intensity per unit mass (MJ/kg)	Energy intensity per unit volume (GJ/m^3)	Ref.
Acrylic	133-175	157-207	Yacout et al. [29], Barber and Pellow [30]
Aramid	-	-	-
Basalt	18	49	De Fazio [31], Inman et al. [32]
Carbon	183-286	309-483	Song et al. [33]
Glass	13-32	34-83	Song et al. [33]
Nylon	250	285	Barber and Pellow [30]
PBO	-	-	-
PE	73-116	71-112	Vlachopoulos [34]
PET	39	53	Yu et al. [35]
PP	75-115	70-108	Barber and Pellow [30]
PVA	101	131	Boustead [36]
Steel	30-60	234-468	Song et al. [33]

Given the high potential of UHPFRC, numerous research has focused on characterizing the response of UHPC under different environmental and loading conditions so as to deepen our knowledge with respect to its behavior.

Yoo et al. [37] studied the flexural performance of UHPC beams reinforced with single and hybrid fibers in overall ratios of 2%. Short steel (SS), medium-length steel (S), end-hooked (H), and twisted (H) fibers were used. Analogies were drawn among various specimens in terms of flexural stress, toughness, and cracking pattern. It was found that SS fiber was more efficient than its counterpart in terms of the investigated parameters. Flexural strengths up to 50.9 MPa were obtained for a 100×100×400 mm beam under 4PBT using this kind of fiber. It was also highlighted that using SS fibers with a length of 19.5 mm and a diameter of 0.2 mm are cost effective than hybrid fibers such as T1.0-S1.0 and T1.0-SS1.0 fibers, the total cost of using each to make 1 m^3 UHPFRC is 509 €, 1022 €, and 1048 €, respectively.

Meng et al. [37] fabricate UHPFRC with an optimized mix design which resulted in 28-day compressive strength of 120 MPa and 165-175 MPa under heat curing conditions for only a day. It was reported that the cost per flexural strength per 1 m^3 of UHPFRC under standard heating conditions was 4.1-4.5$

Dong [38] carried out a study to assess the life-cycle performance, equivalent annual cost, and environmental impact of UHPFRCs. Comparisons were made between NSC and UHPFRC beams with the same reliability index. It was reported that, in terms of sustainability, UHPFRC performs well better than its NSC counterpart. While its production is a bit costly, given that UHPFRC specimens require less maintenance, rehabilitation, and repair, environmental impacts of their usage expressed as the content of CO_2 emission reduced by 48%, therefore having lower global warming impact.

2. Background on Three-Point and Four-Point Bending Tests

There is not a consensus on the flexural loading of beams, particularly notched ones; JCI SF4 [39], NBN B 15 238 [40], Teutsch [41] and ASTM C1399/C1399M [42], recommend unnotched four-point beam tests; RILEM TC 162-TDF [43], DIN EN14561 [44], ASTM C1609/C1609M [45], FIB Model Code [6] and ASTM C293/C293M [46], in contrast, recommend three-point loading tests on notched specimens.

Researchers have attempted to highlight the fracture properties of FRCs over the last two decades. Navalurkar et al. [47] carried out studies to quantify the fracture energy of high-strength concrete; a bilinear relationship between CMOD and mid-span deflection was observed.

Notched steel fiber-reinforced concrete (SFRC) specimens tested by Chiaia et al. [48] under three-point-bending showed that the relationship between CMOD and mid-span-deflection is an intrinsic property of the specimen.

Notched high-strength SFRCs with different fiber contents were incorporated in beams with dimensions of 100×100×515 mm by Zhang et al. [49]. It was reported that CMOD/CTOD ratio was influenced by the fiber content and results indicated that fiber content influences the critical CMOD to crack tip opening displacement for a fixed notch-to-depth ratio. A linear relationship between mid-span deflection and CMOD for SFRCs was also noted by Ding [50].

Plain and fiber-reinforced self-compacting concrete (SCC) beams with four different mix designs and fiber types were tested by Aslani and Bastami [51], resulting in a deflection-CMOD relationship for each mix. Similar to research on other types of concrete, it was observed that load-deflection and load-CMOD curves are identical and a linear relationship governs their behavior.

Various notched UHPC beams with dimensions of 75×75×400 mm were tested by Meng et al. [52] under three-point loading. Notch-to-depth ratios were 1/6, 1/3 and 1/2. Results revealed that residual and flexural strengths increase with the notch-to-depth ratio. What's more, a notable increase in fracture energy (up to 87%) was observed for smaller notch-to-depth ratios and higher deflection values.

3. Experimental Program

3.1. Materials

Cement: Type II Portland cement which is the most common cement for typical applications and is produced by pulverizing clinkers (constituents of which are iron, aluminum, and siliceous oxides were used [53]). This type of cement produces less heat during hydration when compared to that of type I [54].

Silica Fume and Silica Flour: By-product of the smelting process, this reactive pozzolanic material with a maximum size of 229 nm was utilized in this study. To discard any unwanted particles, sieving was performed. Mix composition of cement and silica fume is given in Table 7.

Table 7. Material composition of cement and silica fume.

	Cement	Silica fume
CaO	61.33	0.38
Al_2O_3	6.40	0.25
SiO_2	21.01	96
Fe_2O_3	3.12	0.12
MgO	3.02	0.10
SO_3	2.30	-
Specific surface area	3413	200,000
Density (g/cm^3)	3.15	2.10

Superplasticizer: In most cases, in order to attain UHPFRC with excellent mechanical properties, low water-to-binder ratios are required which in turn results in reduced workability. To overcome this issue, polycarboxylate-based ethers are utilized in proper amounts. The so-called superplasticizers have the advantage of reducing the amount of water as well as facilitating the mixing process in the meantime. Type "F" HRWRA was used in this study [55].

Silica Sand: Local materials were used as fine aggregates. Fine sand passing from sieve No. 16 (1.18 mm) and left on sieve No. 200 (0.074 mm) was used. Mix composition of materials is given in Table 8.

Table 8. Mix composition.

W/B	Unit weight (kg/m^3)					
	Water	Cement	Silica fume	Silica sand	Silica flour	Superplasticizer
0.2	160.3	788.5	197.1	867.4	236.6	52.6

* Superplasticizer includes 30% solid (15.8 kg/m^3) and 70% water (36.8 kg/m^3)

Steel fiber: Specifications of steel fiber are detailed in Table 9 The fibers have the advantage of delaying the formation of micro cracks and therefore increasing the compressive and tensile strength of specimens. It also noteworthy that according to Hegger and Rauscher [56], UHPFRC is characterized by a linear-elastic behavior up to 90% of its compressive strength. This attribute is advantageous as it decreases deflection values and allows for better simulation of their behavior.

Table 9. Properties of steel fiber

Type	L (mm)	D/W (mm)	f_t (MPa)	E(GPa)
Straight micro steel (MS)	13	0.16	2700	200

*L: Length; D/W: Diameter/Width; f_t (MPa): Tensile strength; E: Modulus of Elasticity

3.2. Compression tests

Compression tests were carried out on 100×100×200 mm cylindrical specimens according to ASTM C39/C39M [57]. Load was applied in a displacement-controlled manner with a rate of 1 mm/min. Three specimens were tested and the average value was used. The average compressive strength was 175 MPa which satisfies the minimum requirement of 150 MPa for UHPC [2].

3.3. Flexural tests

Bending tests were carried out on 100×100×500 mm prismatic beam specimens according to ASTM C1609/C1609M [45] with a clear span of 450 mm, initial notch width of 5 mm, and notch depth of 25 mm. Load was applied in a displacement manner with a rate of 1 mm/min. Reaction forces and mid-span deflection values were recorded using linear variable displacement transducers (LVDTs) which has been used by third author in previous works [58-60]. Average flexural load-deflection curve was used as a reference.

4. Numerical Simulation

Despite the superior properties of UHPFRC in comparison to normal concrete, fabrication of this cementitious composite is physically demanding as low water-to-cement is required to produce it. Furthermore, experimental works are costly and time-consuming. Nonetheless, with the advancement of technology, computer simulations are used nowadays to assess the sensitivity of particular parameters of interest, obviating the need for additional experiments. In this regard, finite element software namely ATENA along with the GID [61] pre-processor was used to simulate the flexural behavior of UHPFRC beams in tension. This software has especially been built to simulate the behavior of concrete structures and has been used in the past by numerous researchers to simulate the behavior of normal concrete [62-64] and FRC [65-67]. Some other researchers [68,69] used another software.

It should be highlighted that, despite a tremendous increase of attention toward this class of cementitious composites, few general guidelines are available in the literature (i.e., AFGC [4]) such that there is not a unified approach. Moreover, direct tension tests are difficult to carry out as creating a uniform stress state under uniaxial tension is challenging. For this reason, four-point bending and 3PBT are usually utilized to assess the flexural capacity of the beams, the results of which are used in subsequent using inverse analysis to obtain the tensile curve of the UHPFRC beams.

4.1. Materials, Mesh, and Solution Methods

In the current study, an approach that simultaneously accounts for the tensile (fracturing) and compressive (plastic) behavior of concrete was utilized [58] Compressive strength, modulus of elastic and first cracking stress, obtained from the results and calculated according to equation (1) were used as input parameters. Linear-elastic steel plates with a thickness of 20 mm were simulated to serve as supports (the beam was simply-supported) and loading plates. hexahedral elements with eight nodes, were used to mesh the steel loading plates and supports as well as concrete. "*Displacement for point*" condition was used to apply the load in a displacement-controlled manner with an increment of 0.1 mm per each loading step until failure. Monitors were defined to record the deflection values, crack width values at the bottom of the face, and mid-span deflections.

It should be highlighted that ATENA [61] is capable to give crack widths just by assigning the "*crack width monitor*" to the desired element. In spite of the fact that a crack is considered as a displacement continuity, it is capable of transferring stress

to its other faces. A relationship can, in subsequent, be built between the so-called crack and the traction-separation relationship via the crack opening displacement. To achieve satisfactory results, the crack band model was adopted to reduce reliance on mesh. The band width or otherwise known as characteristic length, L_t is related to the element size as given in equation (1):

$$\varepsilon = \frac{w}{L_t} \tag{1}$$

where ε is the fracture strain; w is the crack width and L_t is the characteristic length. Steps to simulate the behavior of fiber-reinforced composites are as follows:

(1) Input compressive strength, tensile strength, modulus of elastic, and Poisson ratio;

(2) Define the initial tensile function based on the user's experience;

(3) Carry out the analysis, and export load-deflection curves;

(4) Compare the experimental and numerical results. If the obtained result is satisfactory, the analysis is complete. Otherwise, find the crack width values at deflection values where the difference between the two curves is questionable and multiply it to the L_t which is usually taken equal to the mesh size to obtain ε

(5) Interpolate the obtained ε in the initial tensile function curve and modify the corresponding stress value by multiplying it to the ratio of experimental-to-numerical load value.

(6) Perform the analysis with the modified tensile function and follow steps (4)-(6) until satisfactory results are obtained. It is noteworthy that the precision of the resulting

flexural load-deflection curve depends on the number of iterations and the accuracy desired by the user.

It is noteworthy that the tensile strength and modulus of elasticity of UHPFRC was estimated based on the equation given by Wille et al. [15] and Suksawang et al. [70] as expressed in equations (2) and (3):

$$\sigma = -\left(V_f - 4\right)^2 + 14 \tag{2}$$

$$E = 4700\lambda\sqrt{f_c'} \quad \lambda = (1 + 0.7^{V_f})/2 \tag{3}$$

where σ is the tensile strength; V_f is the volumetric content of steel fibers; E is the modulus of elasticity of fibrous concrete; f_c' is the compressive strength of concrete and λ is a parameter depending on V_f. Finite element mesh, tensile function, and comparison of experimental and numerical flexural load-deflection curves are given in Fig. 2. It can be observed that results are in good agreement with one another. It is noteworthy that "*fixed contact*" in Fig. 2 (a) follows the master-slave concept, and "*constraint*" means support. It is the terminology used in the ATENA-GID interface. Furthermore, cracking pattern of specimens are shown in Fig. 2 (e)-2(h).

4.2. Parametric Analyses

4.2.1. Mesh Size, and Compressive Strength

Results of the mesh sensitivity analyses given in Fig. 3 indicate that finer mesh leads to stiffer results in the post-response of the load-deflection/CMOD/CTOD beams. It should be mentioned that "*M10*" denotes a mesh size of 10 mm, and *N5D25*: notch width of 5 mm, notch depth of 25 mm. The difference, however, is negligible. The same observation is valid for the variations in the compressive strength (Fig. 4).
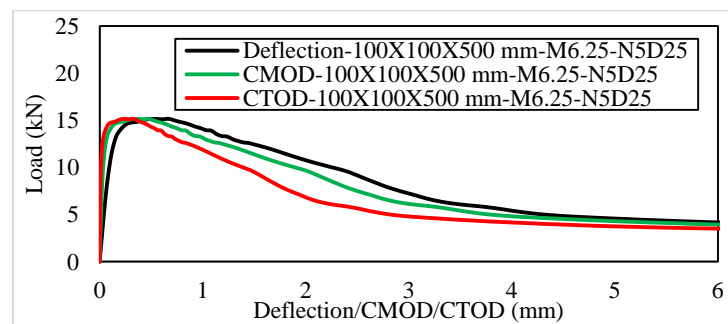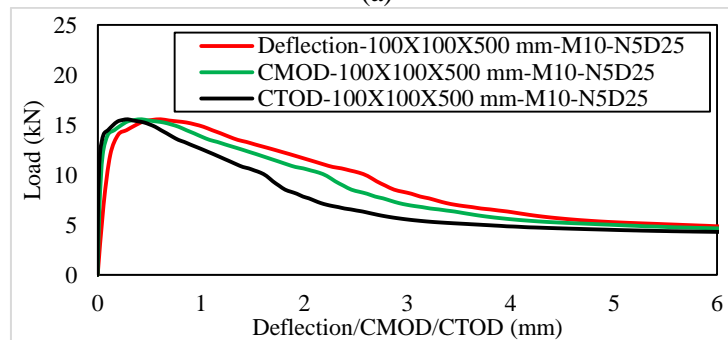
(a)

(b)

(c)

(d)

(e)

(f)

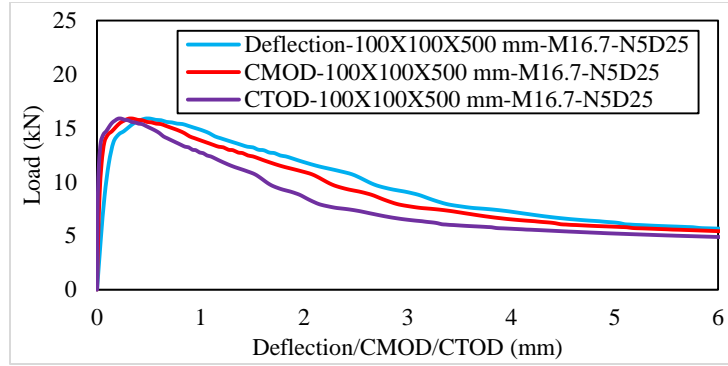(g)   (h)
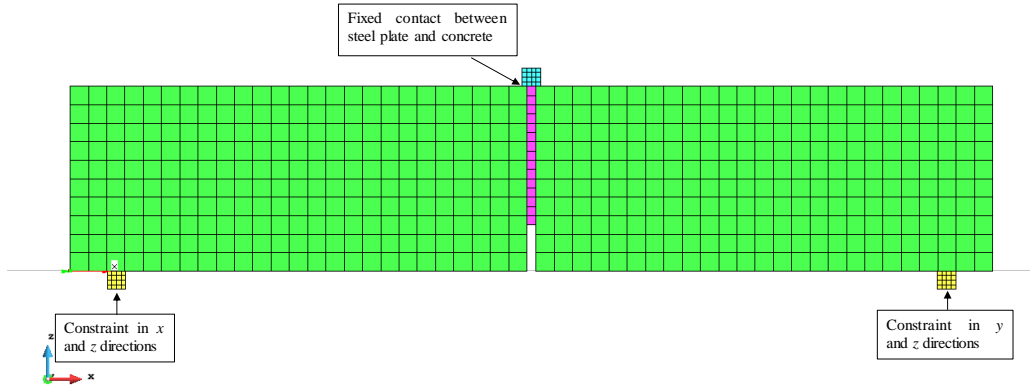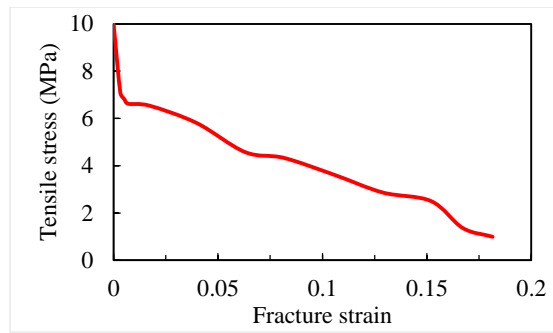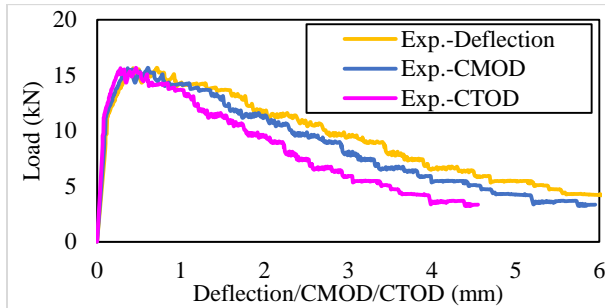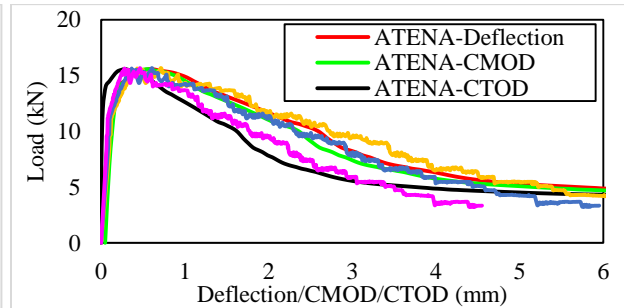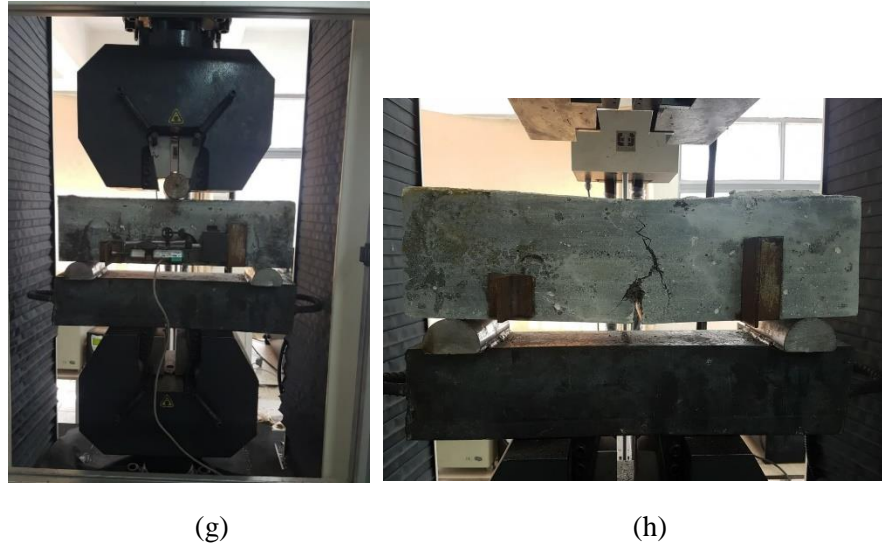
Fig. 2. (a) Finite element mesh and boundary conditions, (b) Post-cracking tensile function (c) Load vs. Deflection/CMOD/CTOD curves, (d) Comparison of numerical and experimental results, and (e)-(h) cracking pattern in unnotched and notched specimens.
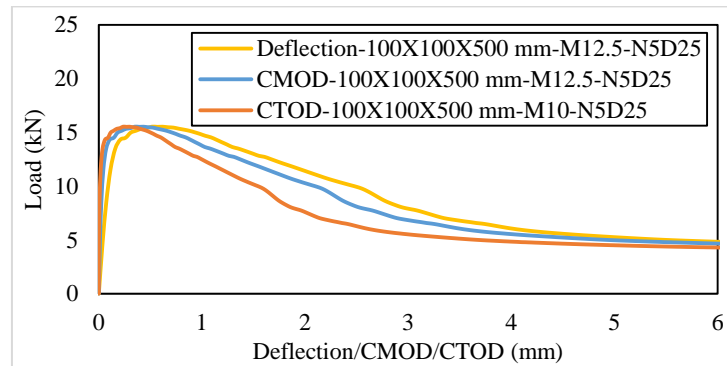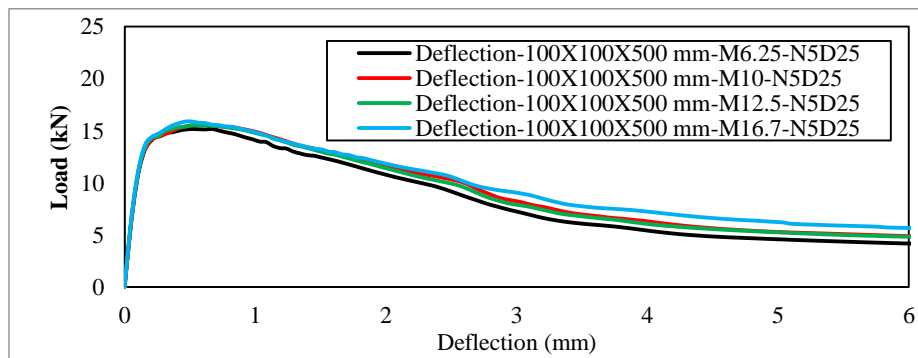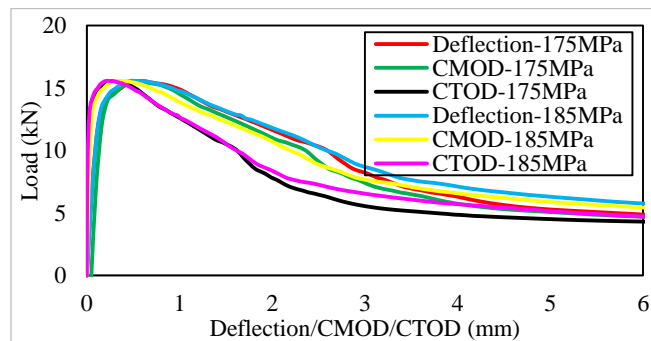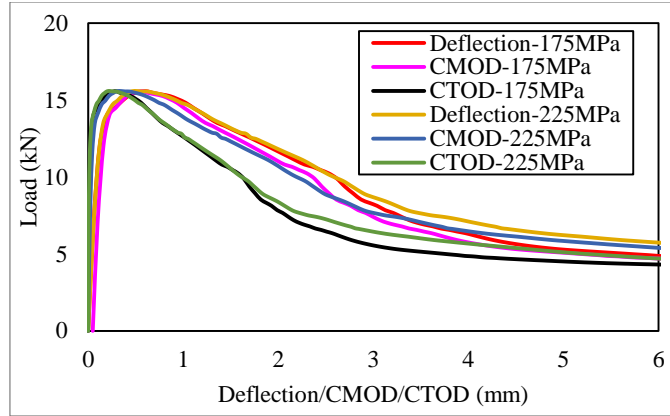

(a)

(b)

(c)

(d)

(e)

Fig. 3. Sensitivity of the load-deflection response to the size of mesh over the height (a) Mesh 6.25 mm, (b) Mesh 10 mm, (c) Mesh 12.5 mm, (d) Mesh 16.7 mm, and (e) comparison of various mesh sizes.

(a)

(b)

Fig. 4. Sensitivity of the model to the compressive strength (a) 185 MPa, and (b) 225 MPa (reference strength: 175 MPa).

4.2.2. Tensile Strength and Modulus of Elasticity

Increasing the tensile strength from 9 MPa, to 14 MPa, resulted in 47% higher stress in the specimen (Fig. 5). while this finding was not true for modulus of elasticity, increasing of which by 25% led to negligible increase of initial slope and post-peak response of the beams (Fig. 6).
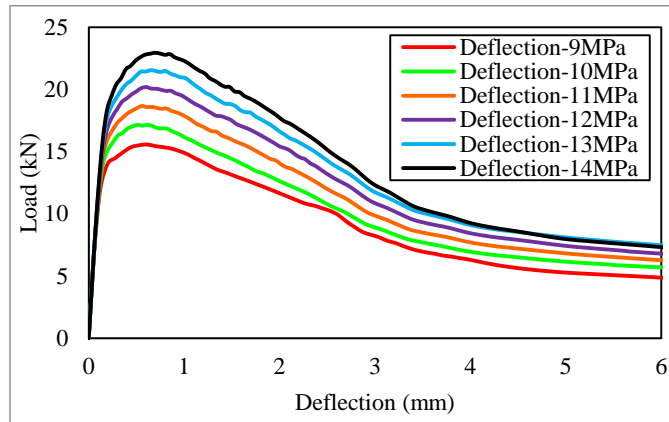
(a)
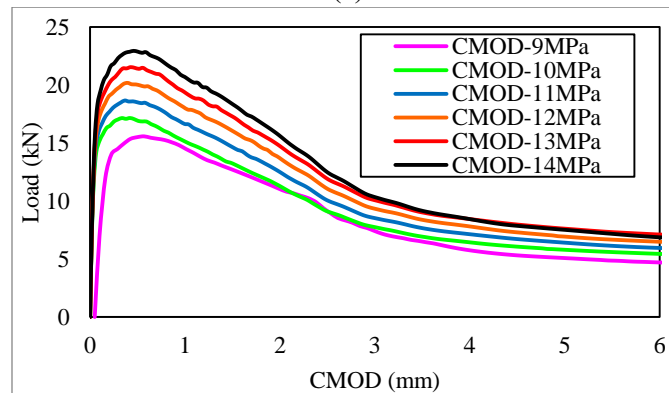
(b)
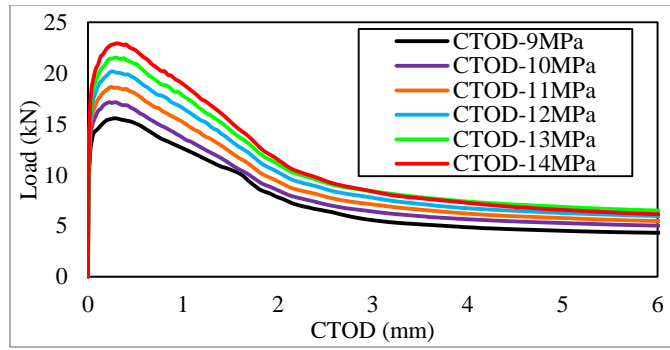
(c)

Fig. 5. Sensitivity of the model to the tensile strength (a), (b), and (c) comparison of load-deflection, load-CMOD, and load-CTOD models with various tensile strengths (reference strength: 9 MPa)
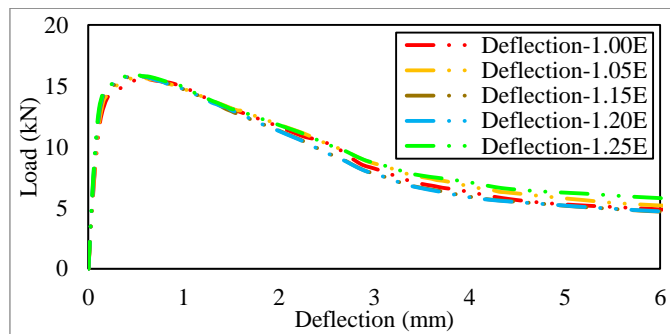
(a)
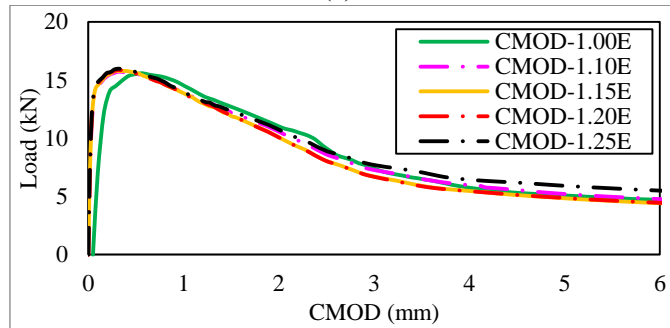
(b)
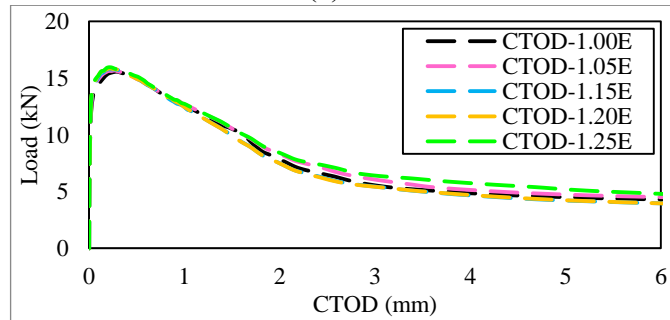
(c)

Fig. 6. Sensitivity of the model to the modulus of elasticity (a), (b), and (c) comparison of load-deflection, load-CMOD, and load-CTOD models with various moduli of elasticity strengths (reference value: 1.00 E)

4.2.3. Effective Depth, Clear Span, Width, and Overall Size

Changing the effective depth from 75 mm to 187.5 mm led to a notable decrease of the deflection corresponding to the peak load (60%) and a marginal decrease in the maximum stress value (9%) which is known as the size effect phenomenon. Likewise, changing the clear span from 450 mm to 900 mm increased the sustained stress by 5.5 % while an increase of 20% in the peak deflection was observed. Unlikely, variations in the width of the beam had almost no effect on the level of the stress, the increase of which up to 150 mm, led to 24% decrease in the peak deflection. For a fixed notch geometry, increasing the effective depth from 75 mm to 187.5 mm, led to a significant improvement of the maximum sustained stress by 7.18 times and 66% decrease in the peak deflection. Overall size variations up to four times relative to the experimental specimen resulted in 16% decrease in the stress value while increasing the peak deflection by 70%. In other words, maximum stresses occur at larger deflection values which is a measure of ductility. The foregoing results which are given in Figures 7-11 and Table 10, were true for each respective load-deflection/CMOD/CTOD responses.
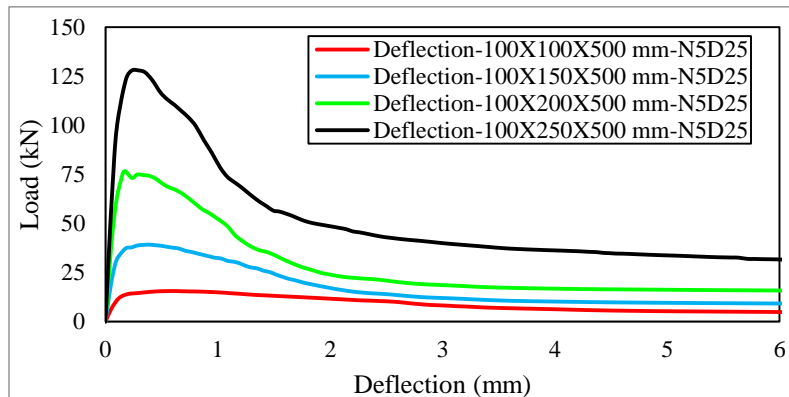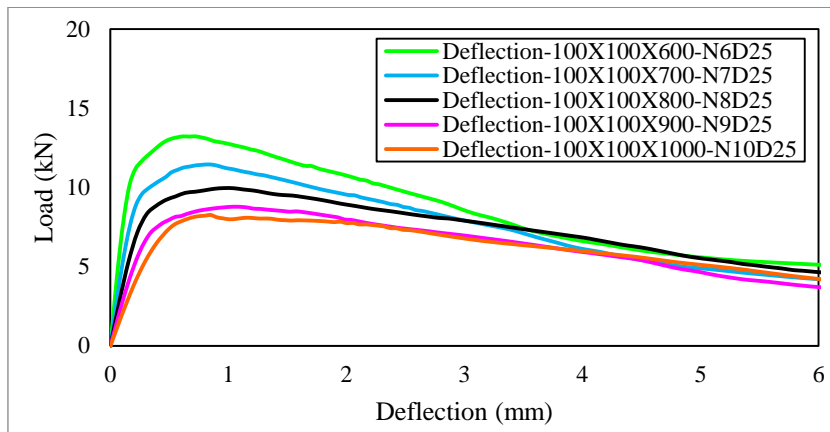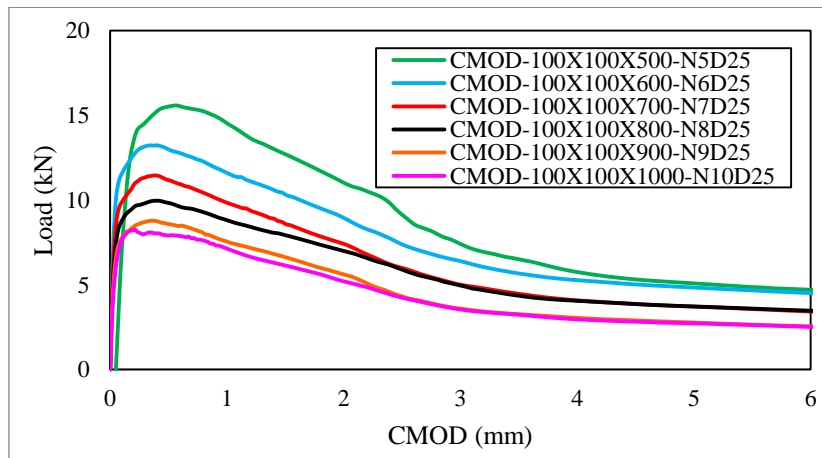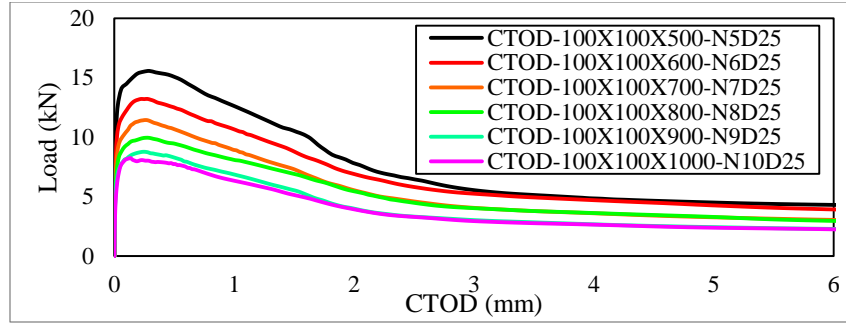

(a)
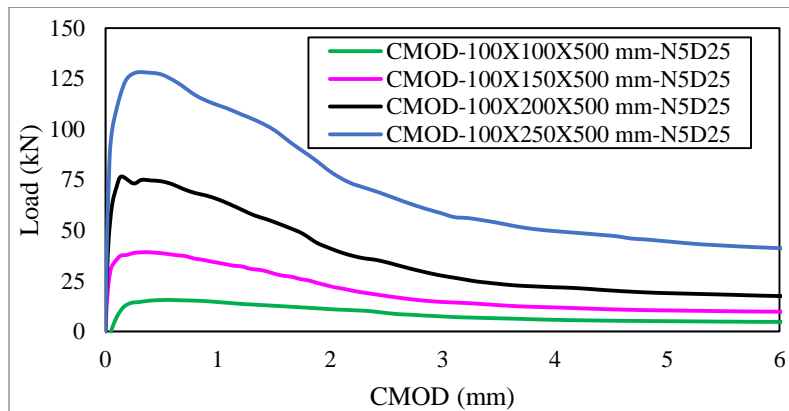
(b)
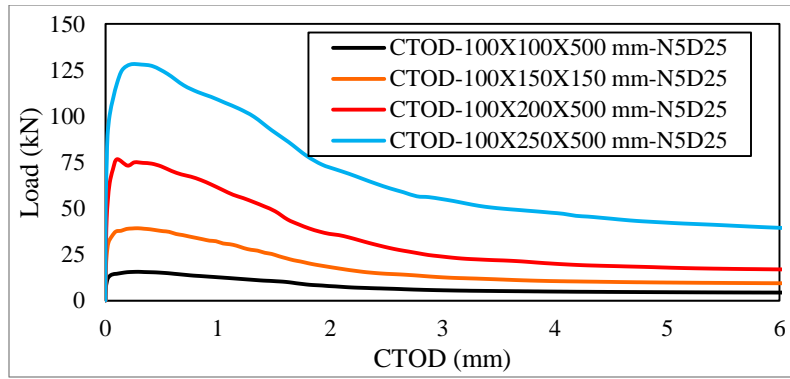
(c)

Fig. 7. Sensitivity of the model to various depths of the notch (a), (b), and (c) Comparison of load-deflection, load-CMOD, and load-CTOD curves with various depths of the notch (reference depth: 25 mm)
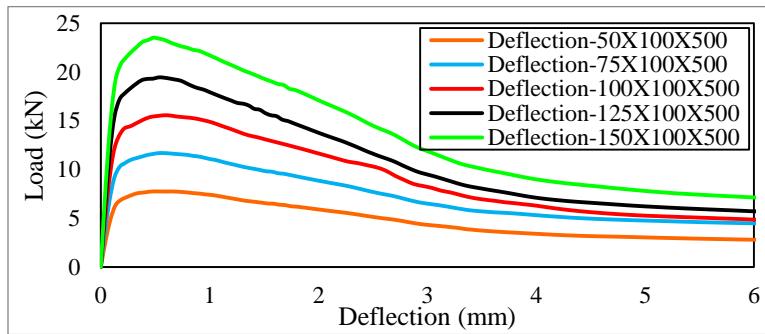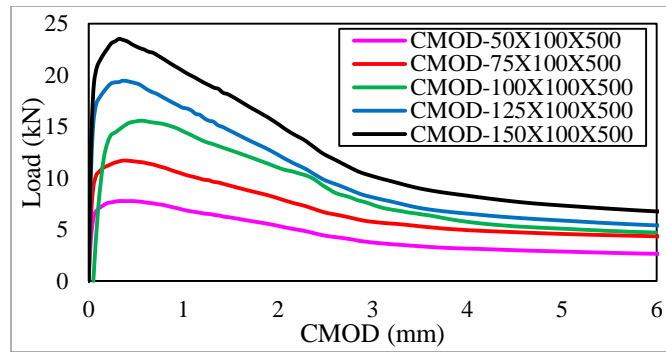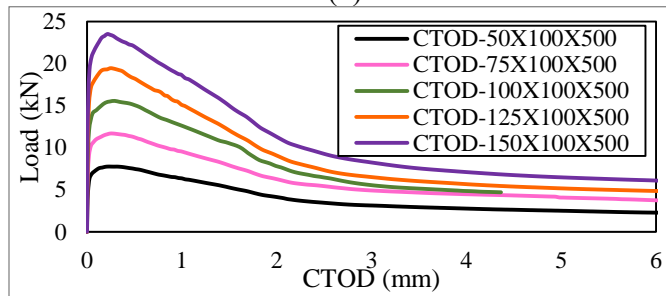

(a)

(b)

(c)

Fig. 8. Sensitivity of the model to various clear span lengths (a), (b), and (c) Comparison of load-deflection, load-CMOD, and load-CTOD curves with various clear span lengths (reference length: 500 mm).
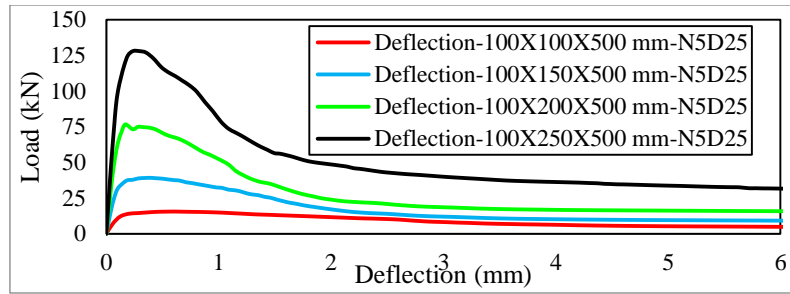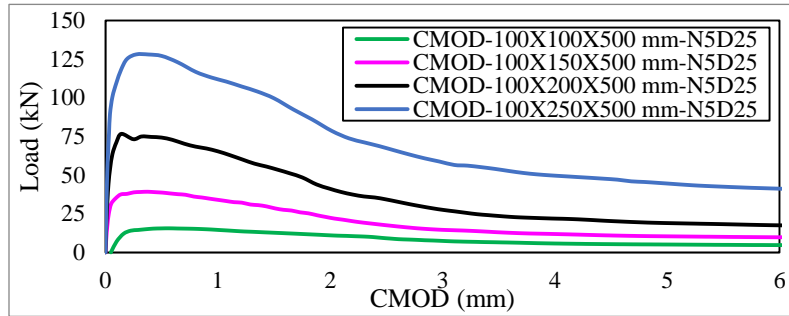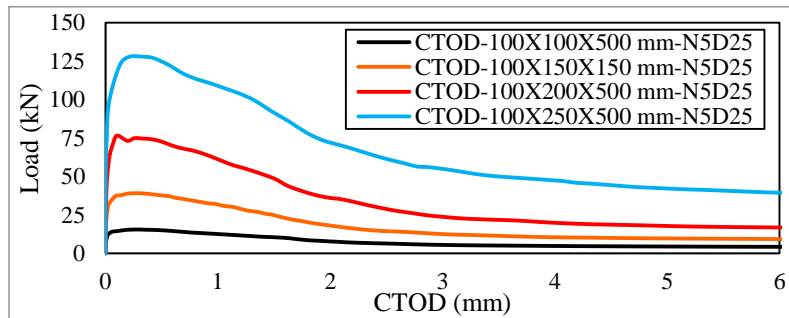

(a)

(b)

(c)

Fig. 9. Sensitivity of the model to various widths of the beam (a), (b), and (c) Comparison of load-deflection, load-CMOD, and load-CTOD curves with various widths of the beam (reference width: 100 mm)

(a)

(b)

(c)

Fig. 10. Sensitivity of the model to various depths of the beam (a), (b), and (c) Comparison of load-deflection, load-CMOD, and load-CTOD curves with various widths of the beam (reference depth: 100 mm)
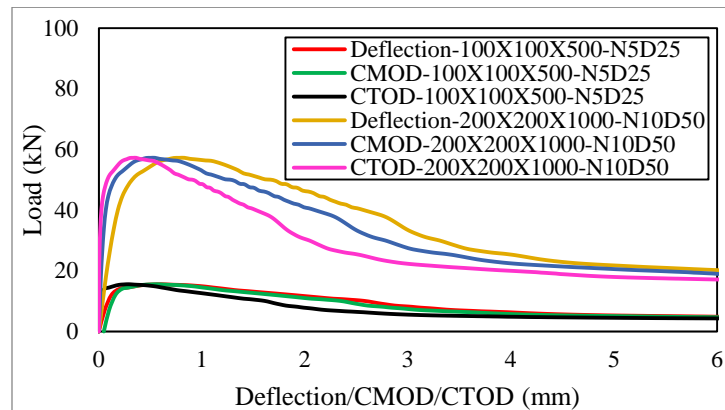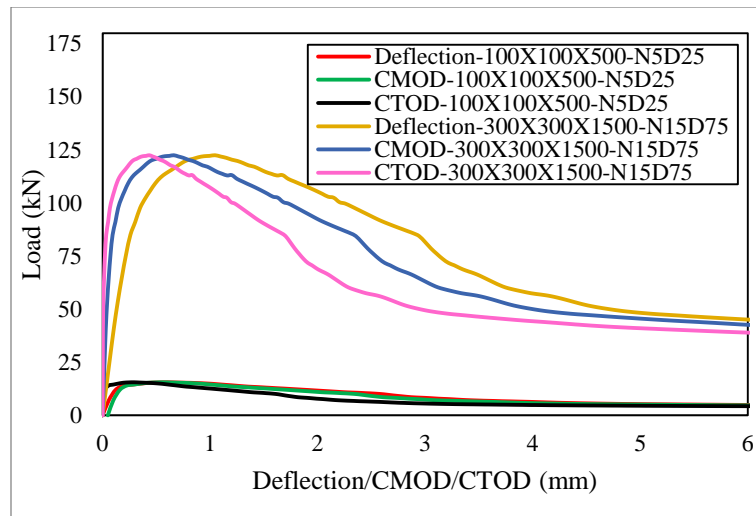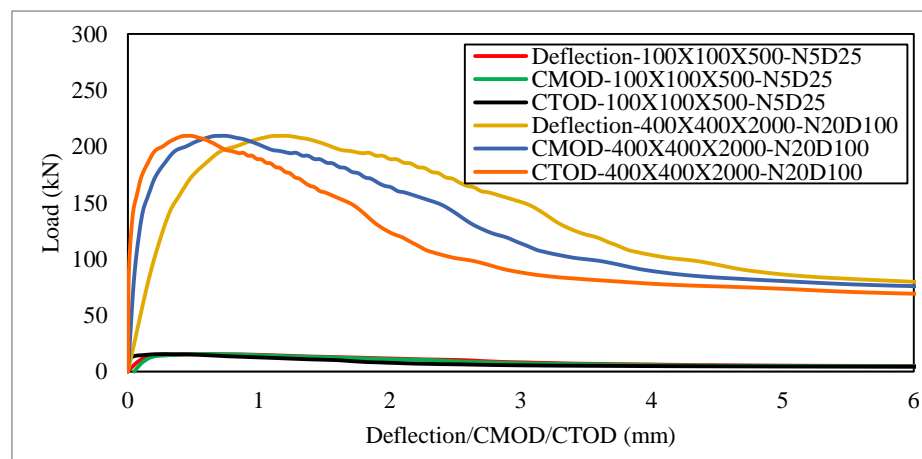

(a)

(b)

(c)

Fig. 11. Sensitivity of the model to overall size of the beam (a) 200×200×1000, (b), 300×300×1500 mm, and (c) 400×400×2000 mm (reference depth: 100 mm)
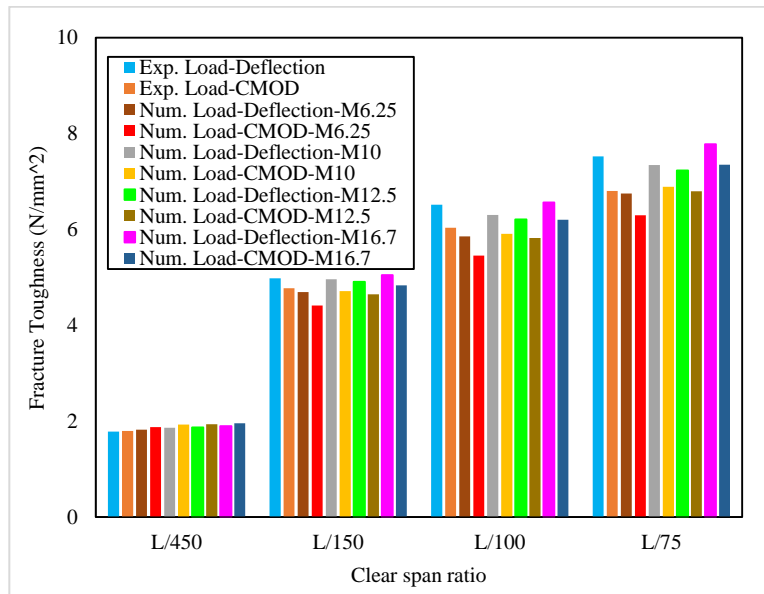
4.2.4. Fracture toughness

Fracture toughness defined as the energy absorbed per effective cross-section of the beam and defined as the area under the load-deflection/CMOD of a notched beam is a property which characterizes the ability of the specimen to resist further cracking under the applied loads. Fig. 12(a)-12(i) show the variation of the so-called parameter with respect to different material properties and geometric considerations. Irrespective of the parameter being investigated, in the pre-peak branch, owing to the stiffer response in the load-CMOD curves, fracture toughness is higher than its load-deflection counterpart while the converse is true for the post-peak branch.

**Table 10.** Numerical and experimental results of specimens.

| Specimen	$\delta_{max}(mm)$	$F_{max}(kN)$	$\sigma(MPa)$	$\dfrac{\delta}{\delta_{Exp.}}$	$\dfrac{\sigma}{\sigma_{Exp.}}$
$50 \times 100 \times 500 - N5D25$	0.494	7.766	12.426	0.695	0.992
$75 \times 100 \times 500 - N5D25$	0.530	11.694	12.474	0.747	0.996
$100 \times 100 \times 500 - Exp. -N5D25$	0.710	15.652	12.522	1.000	1.000
$100 \times 100 \times 500 - N5D25$	0.608	15.581	12.465	0.857	0.995
$125 \times 100 \times 500 - N5D25$	0.484	19.460	12.454	0.682	0.995
$150 \times 100 \times 500 - N5D25$	0.544	23.523	12.546	0.766	1.002
$100 \times 150 \times 500 - N537.5$	0.505	33.066	11.757	0.712	0.939
$100 \times 200 \times 500 - N5D50$	0.362	56.806	11.361	0.510	0.907
$100 \times 250 \times 500 - N5D62.5$	0.285	89.052	11.399	0.401	0.910
$100 \times 100 \times 600 - N6D25$	0.616	13.223	12.694	0.867	1.014
$100 \times 100 \times 700 - N7D25$	0.826	11.449	12.823	1.163	1.024
$100 \times 100 \times 800 - N8D25$	0.962	9.932	12.713	1.355	1.015
$100 \times 100 \times 900 - N9D25$	1.060	8.778	12.640	1.492	1.009
$100 \times 100 \times 1000 - N10D25$	0.850	8.255	13.209	1.197	1.055
$200 \times 200 \times 1000 - N10D50$	0.830	57.249	11.450	1.170	0.914
$300 \times 300 \times 1500 - N15D75$	1.045	122.507	10.890	1.472	0.870
$400 \times 400 \times 2000 - N20D100$	1.211	209.553	10.478	1.705	0.837
$100 \times 150 \times 500 - N5D25$	0.389	39.202	31.361	0.548	2.505
$100 \times 200 \times 500 - N5D25$	0.169	76.621	61.297	0.238	4.895
$100 \times 250 \times 500 - N5D25$	0.239	128.035	102.428	0.336	8.180
$100 \times 100 \times 500 - N5D25 - F_t = 10\ MPa$	0.613	17.154	13.724	0.864	1.096
$100 \times 100 \times 500 - N5D25 - F_t = 11\ MPa$	0.556	18.665	14.932	0.783	1.192
$100 \times 100 \times 500 - N5D25 - F_t = 12\ MPa$	0.515	20.184	16.147	0.726	1.290
$100 \times 100 \times 500 - N5D25 - F_t = 13\ MPa$	0.602	21.541	17.233	0.848	1.376
$100 \times 100 \times 500 - N5D25 - F_t = 14\ MPa$	0.649	22.944	18.355	0.914	1.466

(a)
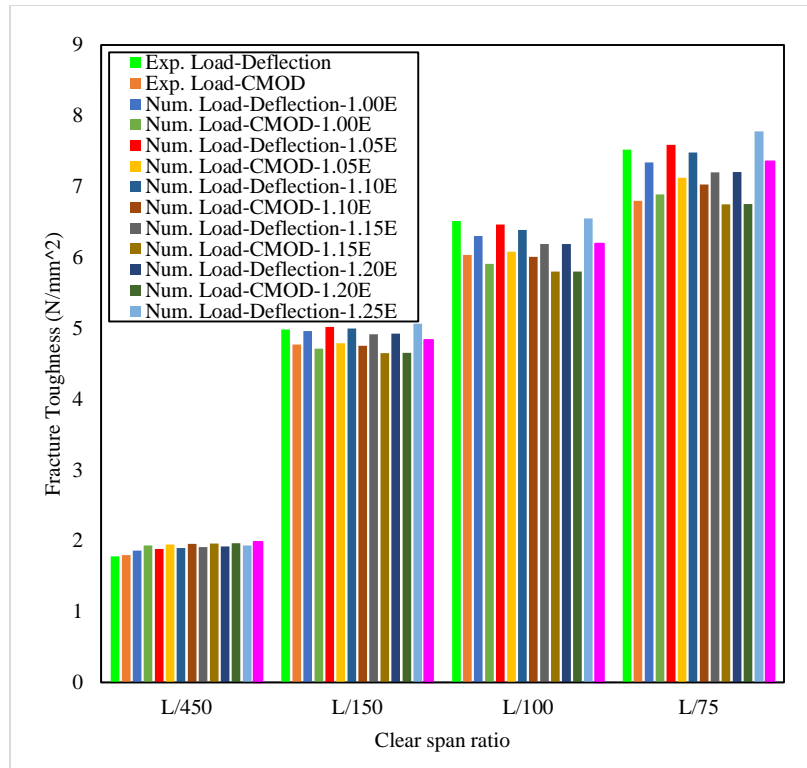
(b)
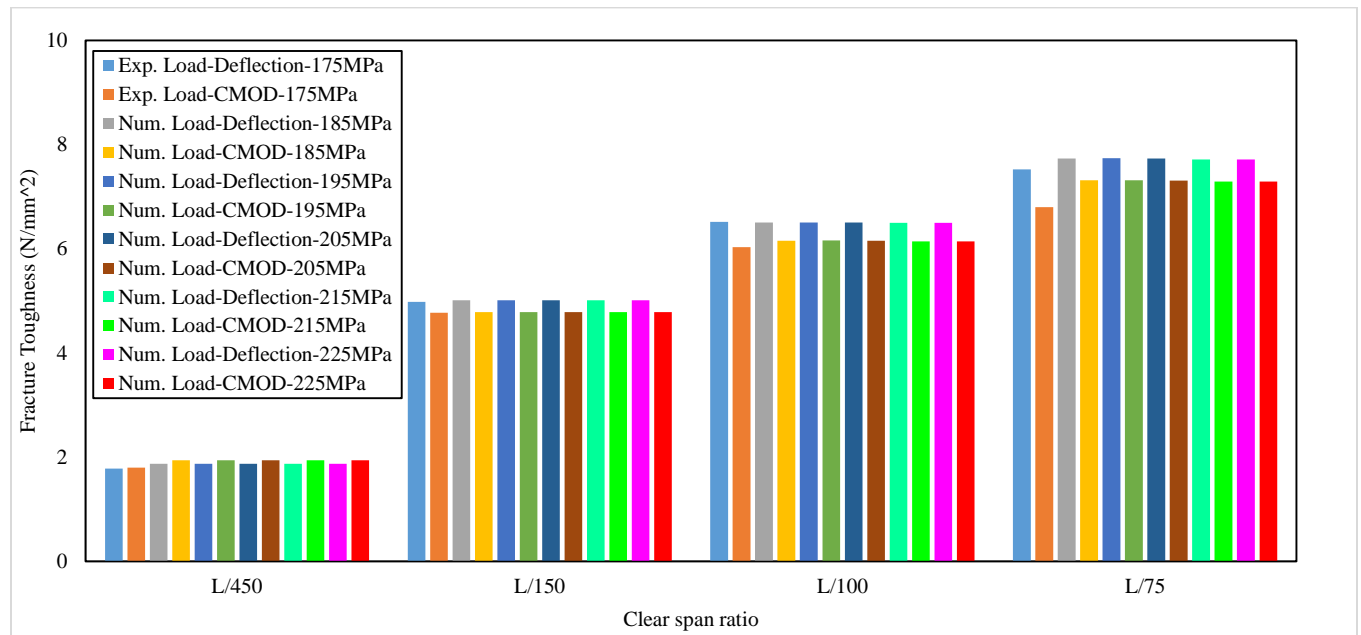
(c)
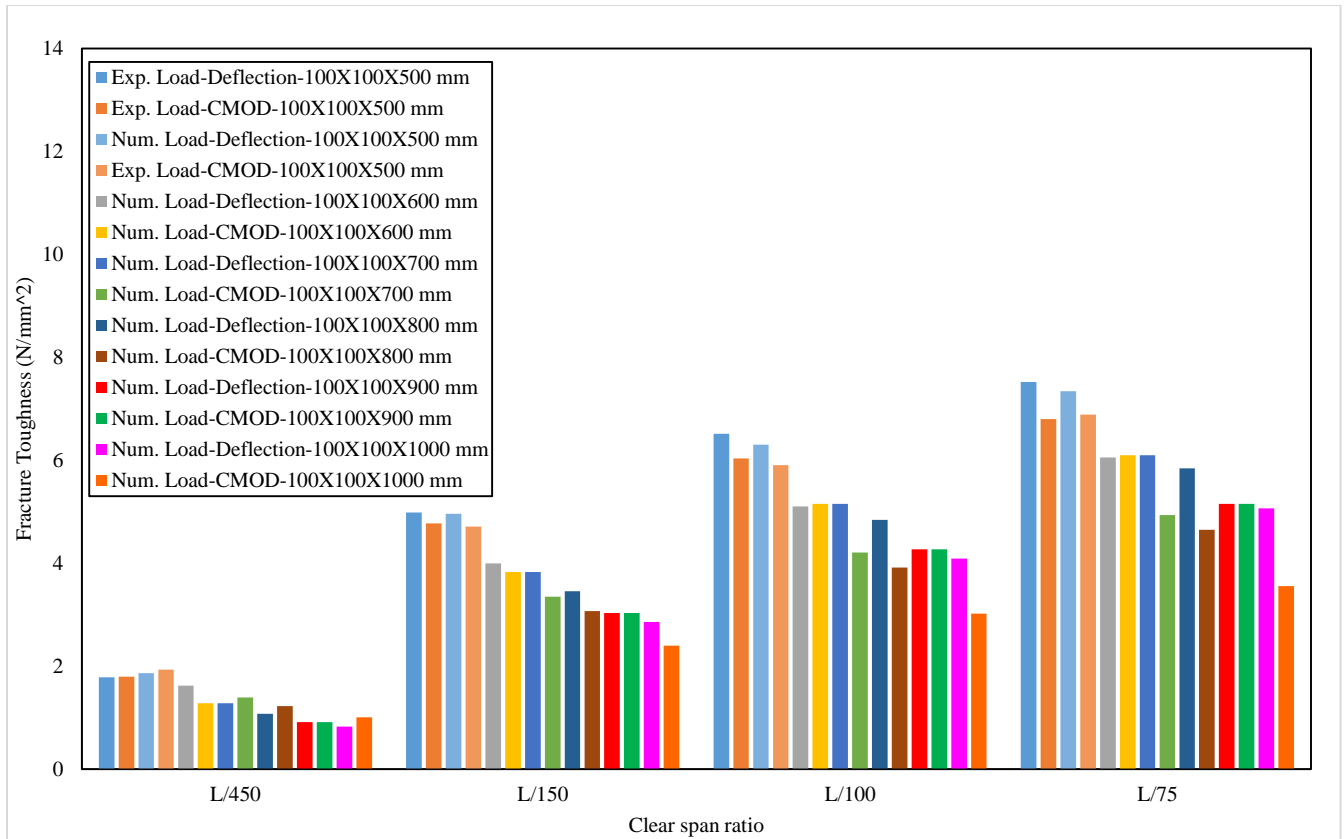
(d)
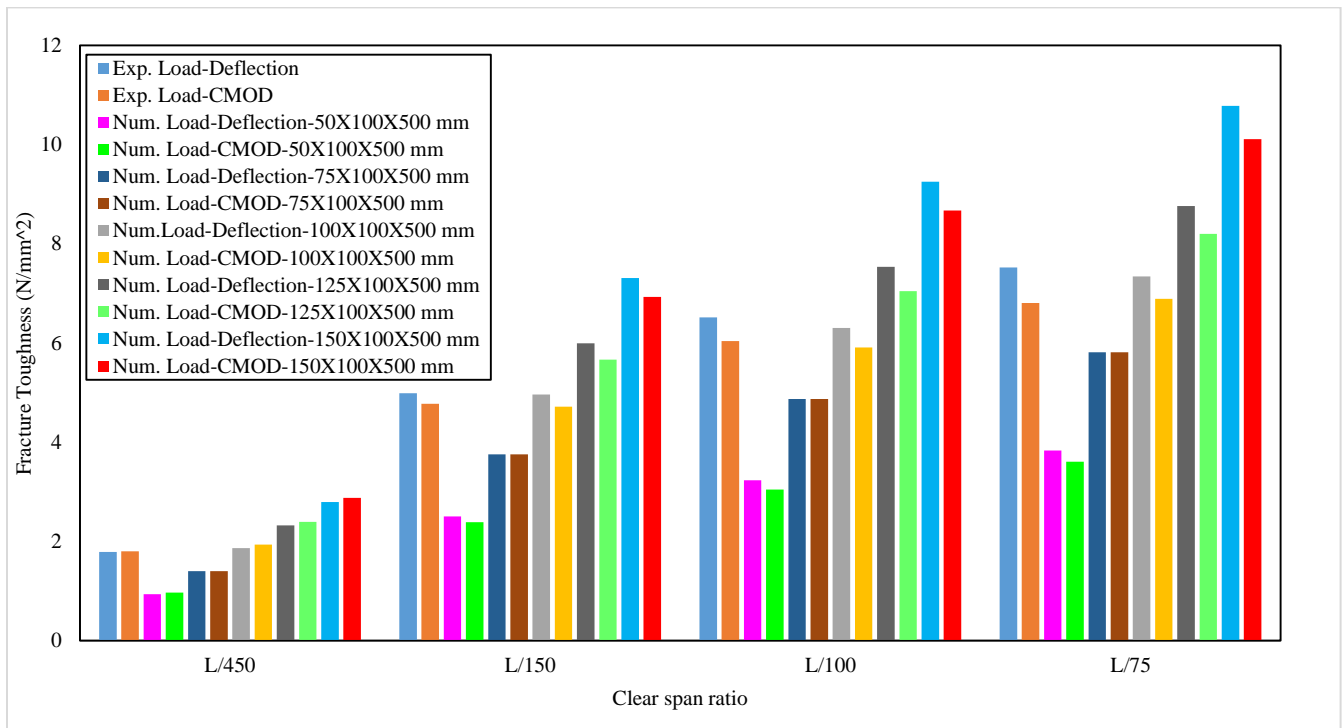
(e)
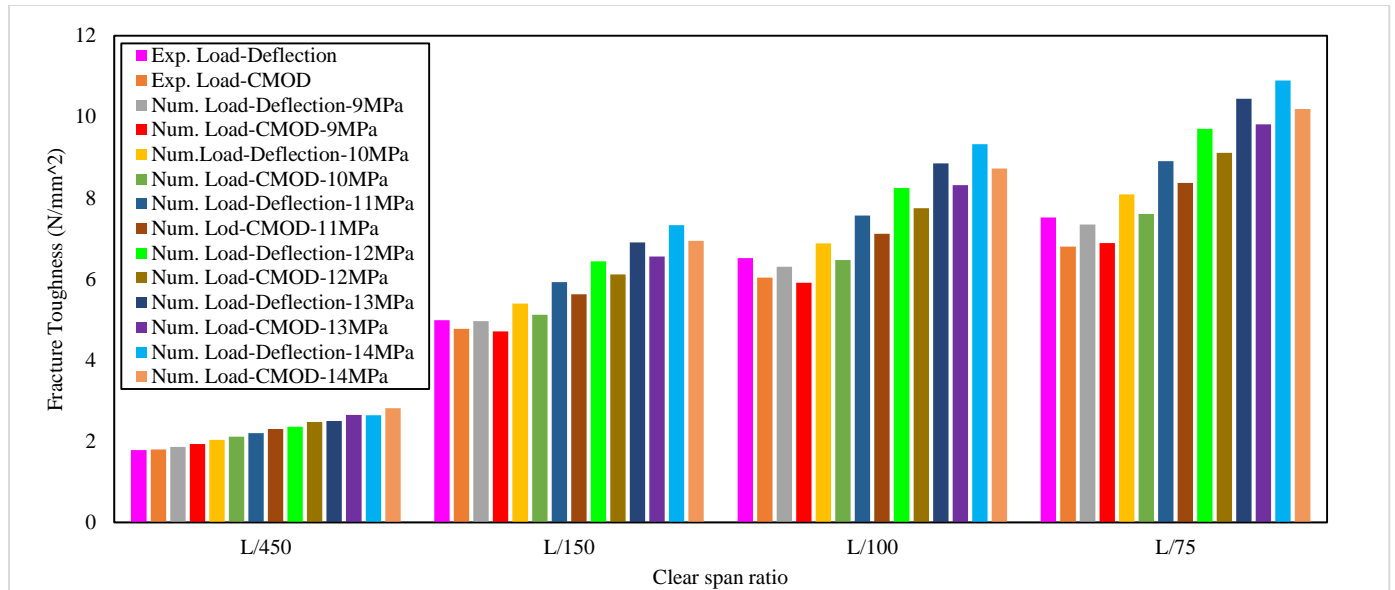
(f)
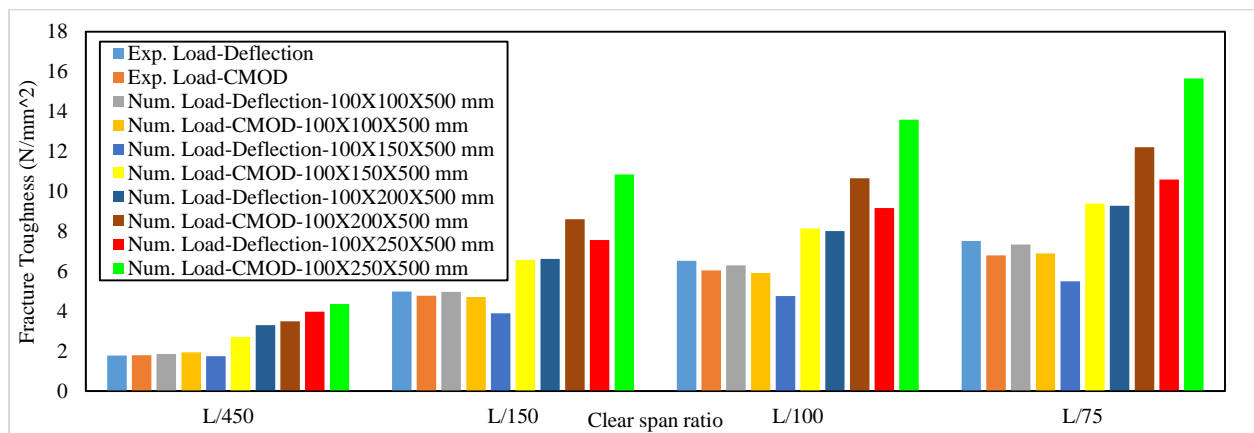
(g)
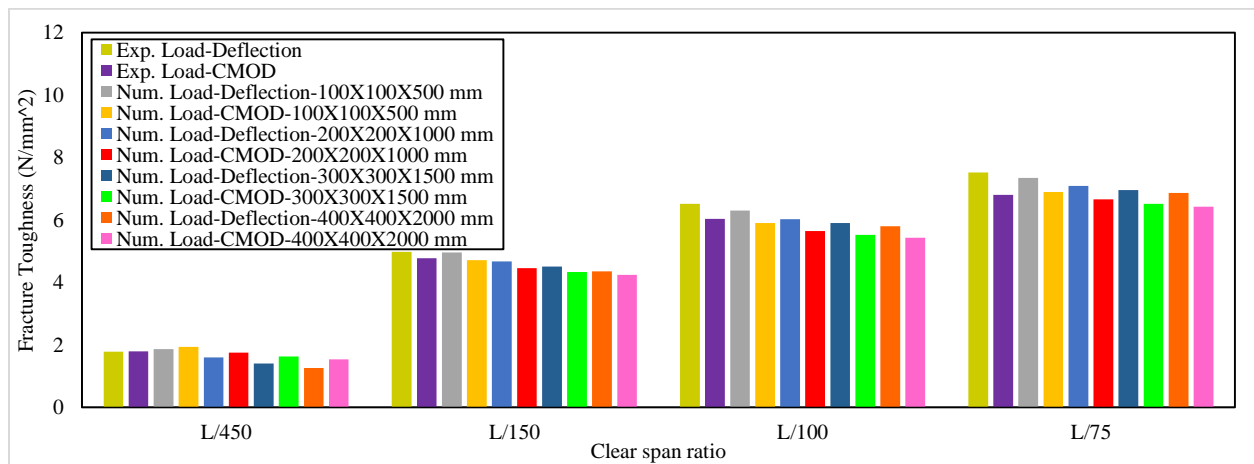
(h)
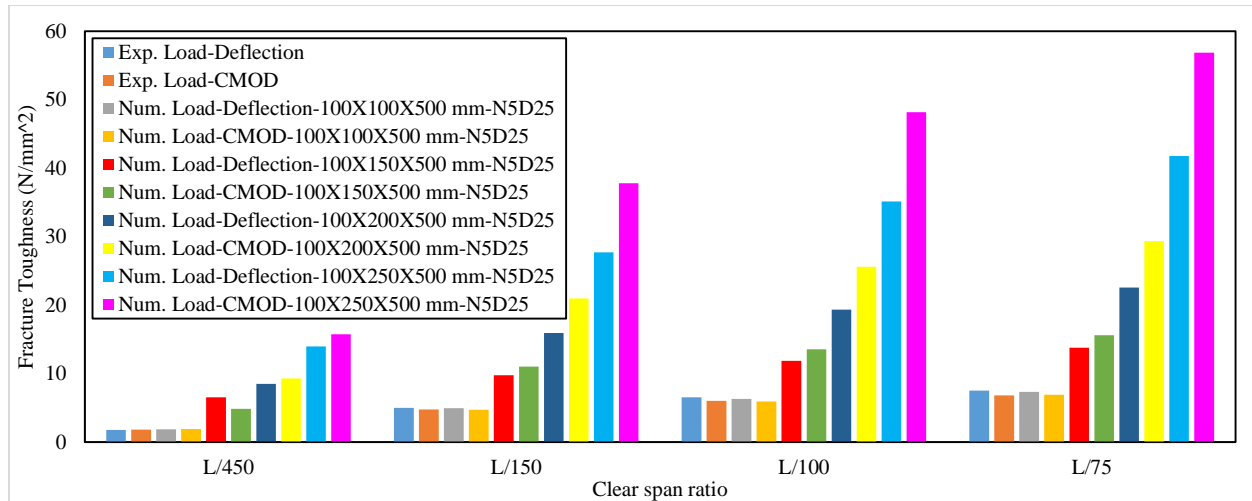
(i)

Fig. 12. Sensitivity of fracture toughness to (a) Mesh Size, (b), Modulus of Elasticity, and (c) Compressive Strength, (d) Tensile Strength, (e) Length of clear span, (f) Width of the beam, (g) Overall size, (h) Height of the beam, (i) Height of the beam at constant notch size

4.3. Deflection-CMOD relationship

According to the literature review given in the introduction, a linear relationship exists between vertical deflection and CMOD. Herein, to provide better insight and draw an analogy with the equations available in the literature, equations (3)-(8) are given as follows:

RILEM TC 162-TDF [43]: $\delta = 0.8475CMOD + 0.0352$ (3)

BS EN 14651 [71]: $\delta = 0.85CMOD + 0.04$ (4)

Ding [50]: $\delta = 0.883CMOD$ (5)

Aslani and Bastami [51]: $\delta = 0.875CMOD + 0.190$ (6)

Almusallam et al. [72]: $\delta = 0.7042CMOD - 0.1211$ (7)

Sadaghian et al. [67]: $\delta = 0.8833CMOD + 0.2828$ (8)

where δ denotes vertical deflection of the beam in the post-peak branch. Results given in Fig. 13 shows the equation proposed by Sadaghian et al. [67] gives the best estimation of the numerical model followed by that of Aslani and Bastami [51], Ding [50], BS EN 14651 [71], RILEM TC 162-TDF [43], and Almusallam et al. [72]. Equations (6) and (7) have an underestimating and overestimating region relative to the numerical model while all the remaining equations overestimate the response with Almusallam et al. [72] giving the highest overestimation.

(a)

(b)

(c)

(d)

(e)

(f)

(g)

(h)

(i)

(j)

(k)

(l)

(m)

(n)
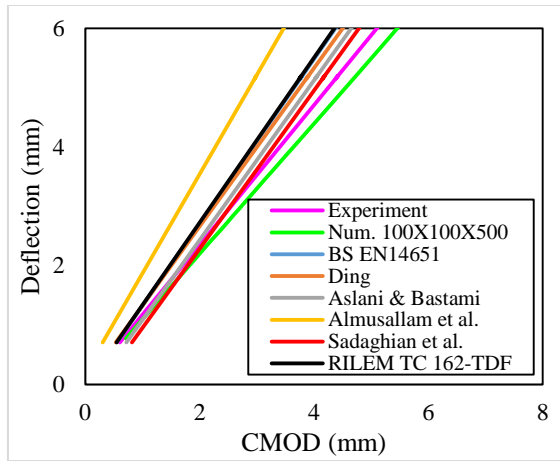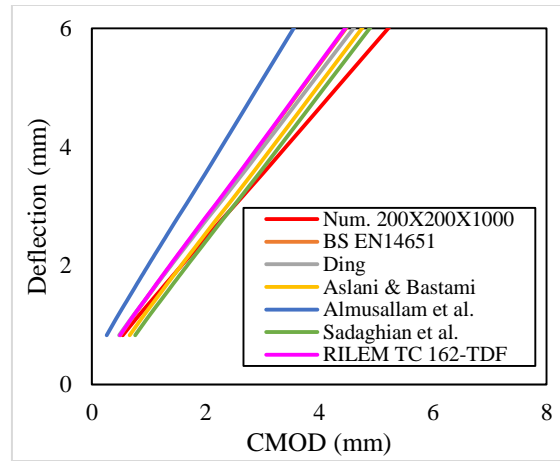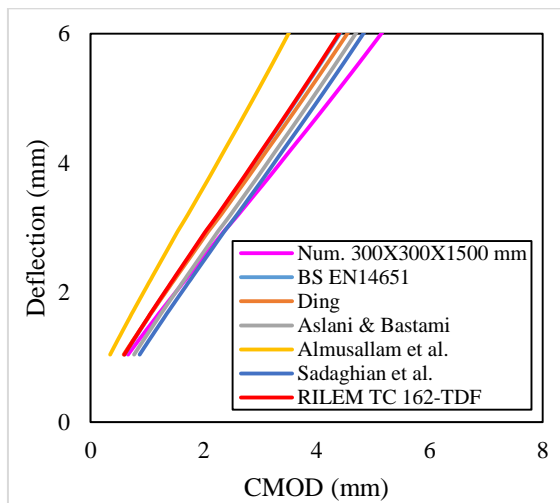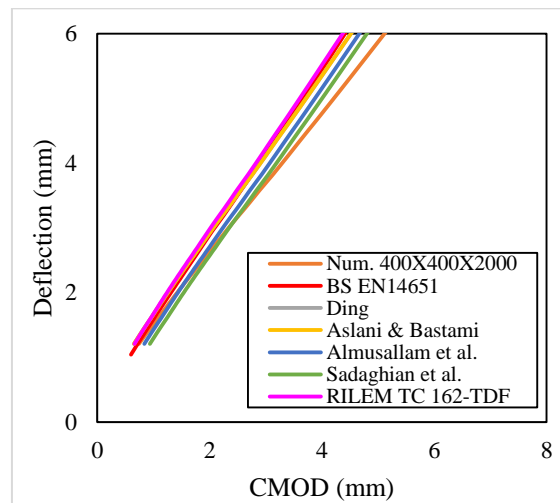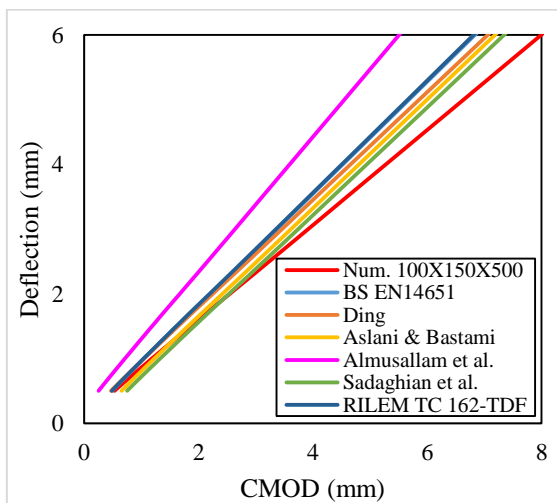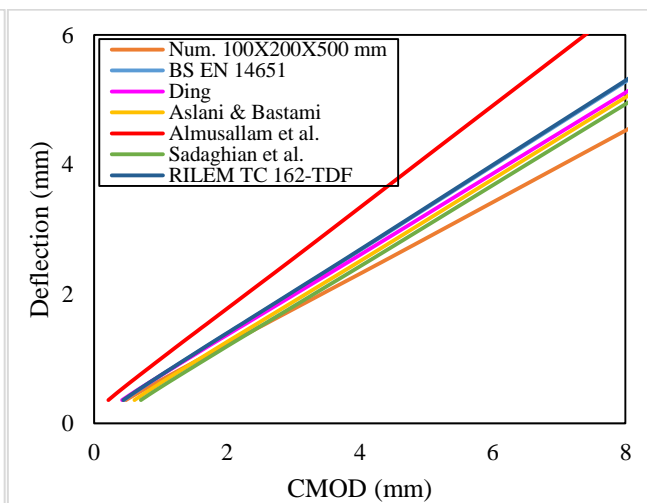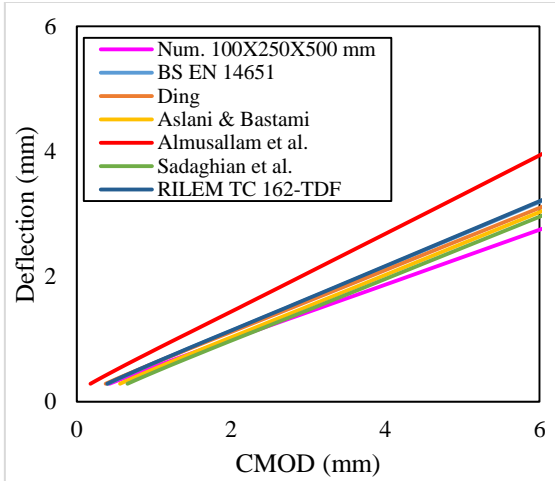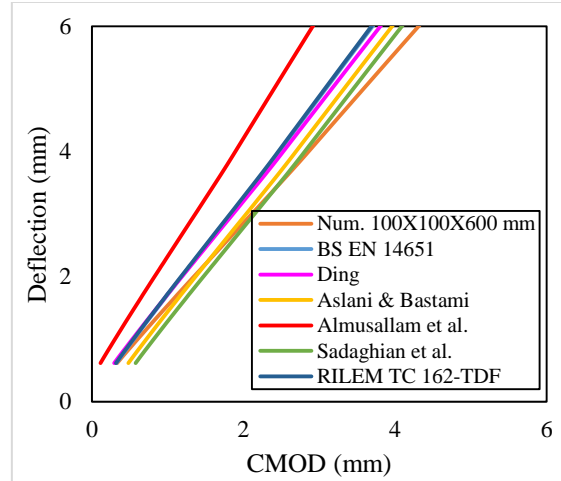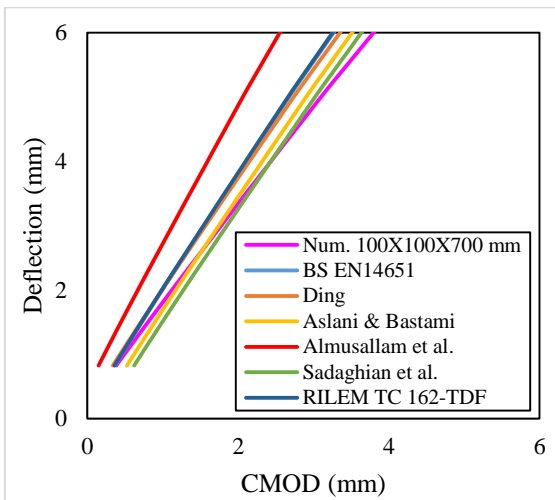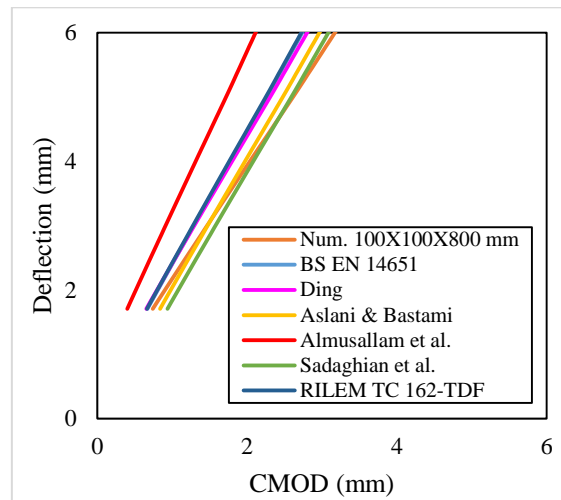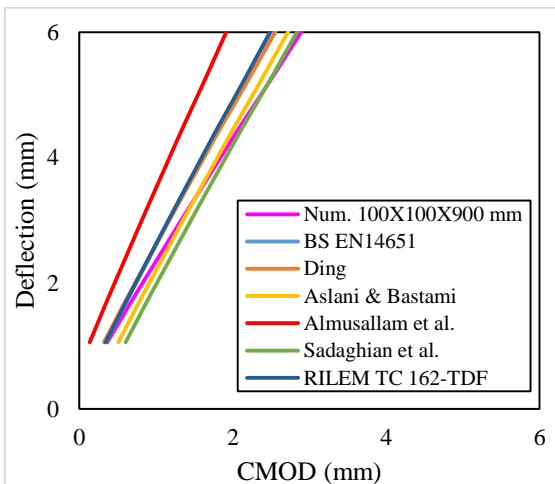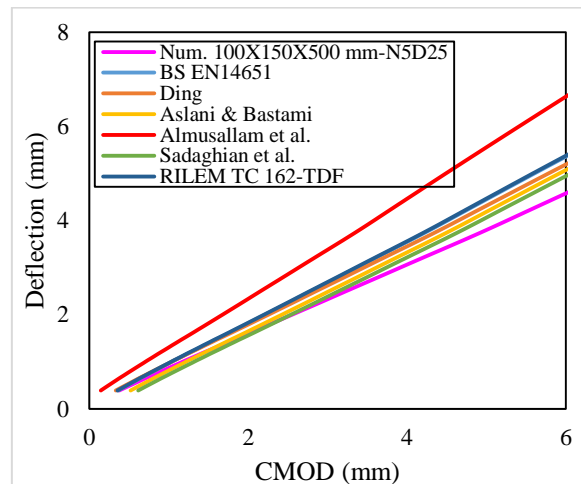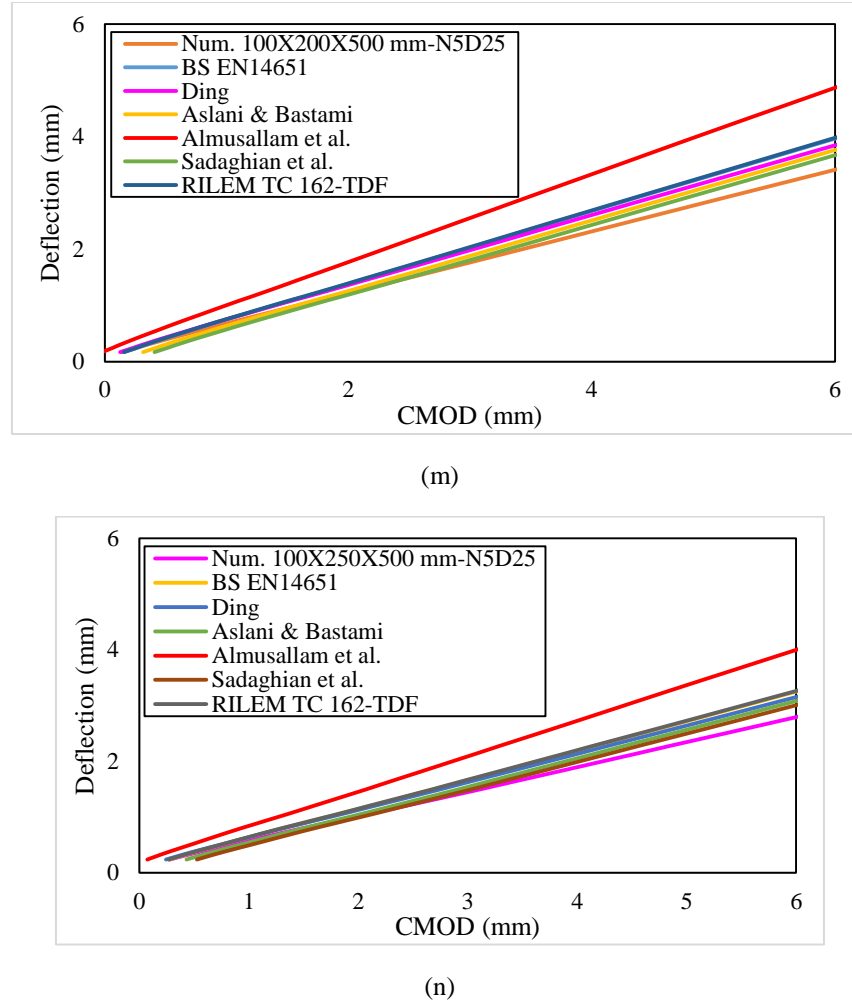
Fig. 13. Comparison numerical deflection-CMOD relationships with available equations in the literature for different geometric considerations

4.4. Modeling of Size Effect

Three well-known theories exist concerning the consideration of size effect: (1) statistical theory introduced by Weibull [73] which correlates size effect to the random nature of material strength, (2) Fracture-based theory put forward by Bazant and Chen [74] (equation (9)) that attribute size effect to the release of fracture energy and stress distribution, and (3) theory proposed by Carpinteri and Chiaia [71] (equation (10)) that establish a relationship between size effect and crack fractality.

Herein, the method given by Bazant and Chen [74] and Carpinteri and Chiaia [75] will be considered as they are suitable for quasi-brittle materials (randomness is not accounted for in this study so the Weibull approach is not utilized). For very large specimens, equation (9) tends to give zero stress results which is not acceptable. Therefore, equation (9) was modified by Kim and Yi [76] according to equation (11).

$$\sigma_N = \frac{\beta f}{\sqrt{1+\beta}}; \quad \beta = \frac{d}{d_0} \qquad (9)$$

$$\sigma_N = F\sqrt{1 + \frac{l_{ch}}{d}} = \sqrt{A + \frac{B}{d}} \qquad (10)$$

$$\sigma_N = \frac{\beta f}{\sqrt{1+\beta}} + \alpha f \qquad (11)$$

where σ_N is the nominal stress; d is the effective depth of the beam; f is the tensile strength of the material; F, l_{ch}, A, d, and α are parameters that can be obtained by fitting experimental results. Fig. 14, clearly show the size effect in beams (i.e., the stress reduces with the increase in size) and Table 11 shows the high correlation of the fitting results with that of the numerical results. Despite not shown in Fig. 14, it can be implied that for very small specimens, the model proposed by Carpinteri and Chiaia [75] is likely to give infinite strengths while the model given by Bazant and Chen [74] show an almost linear trend such that for large specimens, the stress tends to become zero. Moreover, evaluating the sensitivity of equations (9) and (10), given in Fig. 14 (c) and Table 11 shows that high capability of the proposed equations to account for the variations of the tensile strength as well.
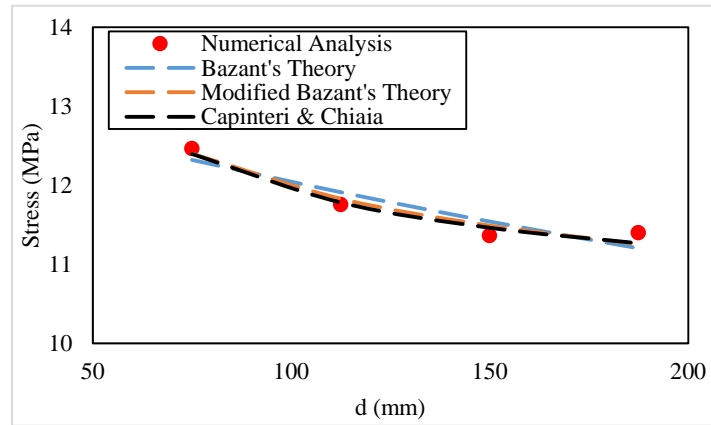
(a)
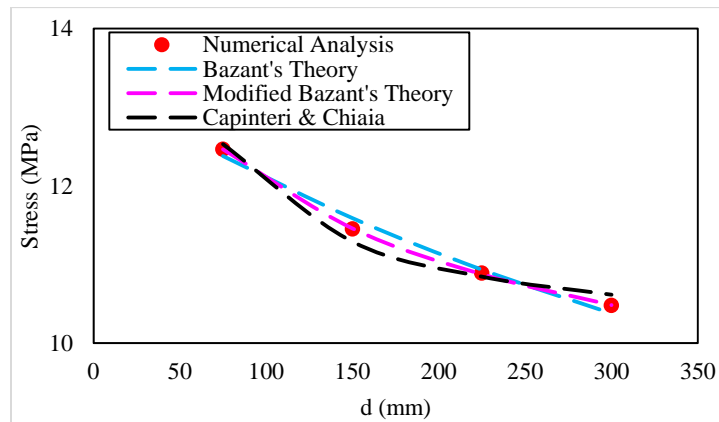
(b)
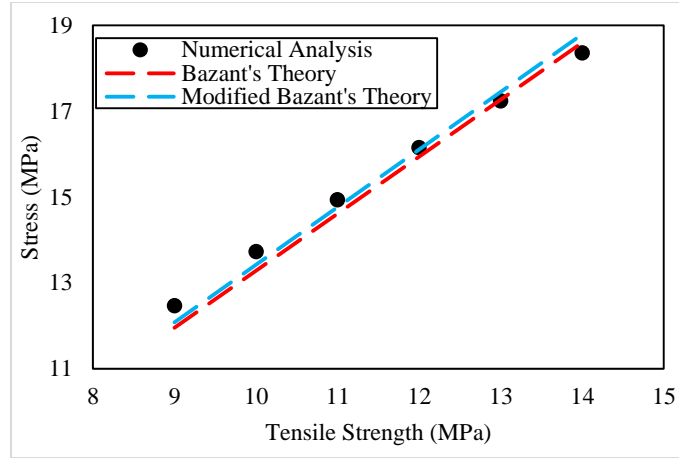
(c)

Fig. 14. Modeling size effect (a) Variable: effective depth≅ notch depth, (b) Overall size, (c) Sensitivity of the models to the tensile strength.

Table 11. Fitting parameters for size effect theories.

Variables	Bazant & Chen [74]			Kim & Yi [76]				Carpinteri & Chiaia [75]		
	B	d_0	R^2	B	d_0	α	R^2	A	B	R^2
Effective depth ≅ Notch Depth	1.4759	462.4333	0.8528	7.3918	0.1645	1.0321	0.9413	109.1580	3338.8122	0.9596
Overall size	1.4838	457.5846	0.9826	0.8481	63.9382	0.8095	0.9999	97.9499	4428.3228	0.9771
Tensile strength	3.6932	11.1411	0.9791	1.5514	2.5812	1.0591	0.9791	---	---	---

4.5. Nonlinear Regression Analysis

It is clear from the foregoing sections that flexural load-deflection curve of a beam is almost linear up to the peak load before descending in a nonlinear manner in the post-peak region until failure occurs. Guo [77] and Yan [78] state that a normalized flexural load-deflection curve should satisfy the following conditions:

(1) for $x = 0$, $y = 0$;

(2) for $0 < x < 1$, the slope of the curve is positive;

(3) for $x = 1$, $y = 1$ at the peak load and the slope is zero;

(4) for $x > 1$, and $\frac{d^2x}{d^2y} = 0$, there is an inflection point in the post-peak branch;

(5) for $x > 1$, and $\frac{d^3x}{d^3y} = 0$, maximum curvature occurs in the descending branch

(6) for $lim_{x\to\infty} x \to y \to \infty$ and $\frac{dx}{dy} \to 0$;

(7) when $x \geq 0$, $0 \leq y \leq 1$.

Based on these attributes, Wang and Xu [79] proposed the equation (12) as follows:

$$y = \frac{ax+bx^2}{1+cx+dx^2} \qquad (12)$$

where a, b, c and d are unknown parameters obtained from regression analyses. Using this

approach, however, is disadvantageous since it has been derived via direct curve fitting which makes the physical meaning of the parameters complicated and the obtained results uncertain. Normalization of both x and y values with respect to that of peak values will resolve this issue, making the obtained curve size-independent and the results more understandable. Based on this explanation, nonlinear regression analysis was carried out on the flexural load-deflection curve and the following relationship (equation (13)) was obtained:

$$y = \frac{a+bx}{1+cx+dx^2} \qquad (13)$$

where $x = \frac{x_{at\ any\ given\ point}}{x_{peak\ load}}$ and $y = \frac{y_{at\ any\ given\ point}}{y_{peak\ load}}$. The results of the regression analysis are shown in Fig. 15 and Table 12. It can be observed that there is very good agreement between the obtained results and the experimental curves with R^2 close to unity. For brevity and similarity of load-deflection and load-CMOD/CTOD curves were not presented. Deviations from the original curve in the descending branch can be justified by the fact then, the overall shape of the curve is governed by the shape of the fiber, mix design, loading setup, etc. A similar approach has also been adopted by Wu et al. [80], Dadmand et al. [65, 66], and Sadaghian et al. [67].
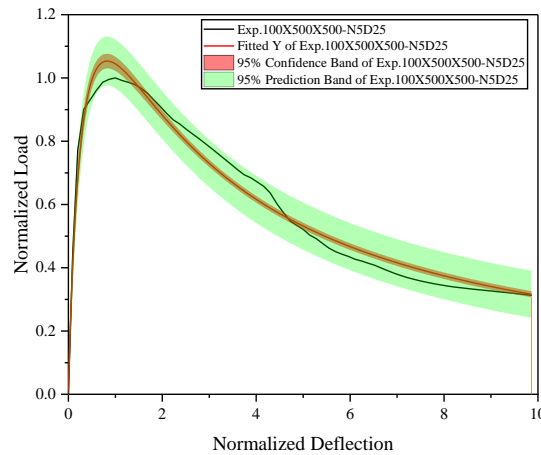
Fig. 15. Typical nonlinear regression curve of normalized load-deflection curve

Table 12. Statistical and ANOVA parameters for nonlinear regression of experimental load-deflection curve.

Specimen		Value	t-value	Prob>|t|	Dependency	Reduced χ^2	R^2	Adj. R^2	F-value	Prob>F
$100 \times 100 \times 500 - Exp. -N5D25$	a (Std.)	0.6144 (0.0132)	46.5737	0.0000	0.9011	0.0019	0.9723	0.9722	31778.1225	0
	b (Std.)	0.6852 (0.0508)	13.4886	0.0000	0.9968					
	c (Std.)	0.0341 (0.0234)	1.4569	0.14560	0.9704					
	d (Std.)	0.2885 (0.0165)	17.4753	0.0000	0.9927					

4.6. Cost analysis

Economic and environmental aspects are an undeniable part of designing 3D concrete structures, which calls for optimizing the structure as much as possible [81-83]. In this regard, and to assess whether the fabricated UHPFRC with an adequate flexural performance is cost effective, a cost analysis was performed. It should be highlighted that, price per cubic meter should not be the sole criterion to assess the cost-effectiveness of UHPFRCs as in short-term NSC is cheaper than UHPFRC while in long-term, given the maintenance, repair, and rehabilitation that NSC requires, UHPFRC proves to a sustainable product which has been asserted by other researchers as well [1]. The cost per kilogram of each component of UHPFRC is given in Table 13. For comparative purposes, the price for short steel fibers in Korea is 3.554 €/kg; the ultra-short fiber used by Skazlic´ and Bjegovic´ [84] was also 3.554 €/kg. Walraven [85] used steel fibers for 3.223 €/kg. It is clear from these figures and Table 13 that, whether for just steel fibers or for each component, the price to cast UHPFRC is lower in Iran.

Table 13. Cost of each component of UHPFRC.

Material	Price per kg (Rials)
Portland Cement	3,500
Silica Sand	1,000
Silica Fume	12,000
Quartz Powder	15,000
Superplasticizer	200,000
Steel Fiber	250,000
Water	Almost free

350,000 Rials = 1 €

5. Conclusions

Flexural properties of UHPFRC beams with 2% micro steel fiber were investigated experimentally and numerically. Numerous parametric analyses were carried out to study the influence of each parameter; Deflection-CMOD findings were evaluated against available equations in the literature; size effect theories were also accounted for. Summary of the findings are as follows:

1- Width, modulus of elasticity, and compressive strength variations have minimal influence on the flexural response of the beam. Tensile strength variations, in contrast, have notable effects with 40% increase leading to 47% improved strength.

2- For the pre-peak branch, Fracture toughness values are higher when measured by the area of the load-CMOD curve rather than the load-deflection curve. The converse is true for the post-peak branch.

3- Equation poposed by sadaghian et al. (2021) gives the best estimate of the load-CMOD response of the beams while most of the other equations overestimate the response (except for that of the Aslani and Bastami (2015) which aslo provide good estimations).

4- Quadrupling the overall size of the beam leads to to 16% lower bending stress and 70% larger peak deflection; doubling the clear span, values equal to 5.5%, and 20% were obtained for the foregoing parameters.

5- Nonlinear regression equation was proposed which captured the load-deflection curve of the specimen. The findings can be easily etended to load-CMOD, and load-CTOD curves due to their similarity.

6- Cost analysis whas performed to investigate the cost of UHPFRC fabrication per 1 m^3. It was found that the cost to cast UHPFRC is lower in Iran when compared to other countries.

References

[1] Du, J., Meng, W., Khayat, K. H., Bao, Y., Guo, P., Lyu, Z., ... & Wang, H. (2021). New development of ultra-high-performance concrete (UHPC). *Composites Part B: Engineering*, 109220.

[2] SETRA (Service d'études techniques des routes et autoroutes), and AFGC (Association Française de Génie Civil), (2002) 'Ultra High Performance Fiber – Reinforced Concretes- Interim Recommendations (Bétons Fibrés à UltraHautes Performacnes – Recommandations Provisoires), France.

[3] ACI 239 (2012). Committee on Ultra-High-Performance Concrete, American Concrete Institute, Farmington Hills, MI, US.

[4] FIB (fédération internationale du béton), (2013). Model Code for Concrete Structures. International Federation for Structural Concrete, Ernst & Sohn, Lausanne, Switzerland.

[5] BS EN 206:2013+A2 (2021) Concrete. Specification, performance, production and conformity. British Standards Institute.

[6] Richard, P., & Cheyrezy, M. (1995). Composition of reactive powder concretes. *Cement and concrete research*, *25*(7), 1501-1511.

[7] Zhang, D., Yu, J., Wu, H., Jaworska, B., Ellis, B. R., & Li, V. C. (2020). Discontinuous micro-fibers as intrinsic reinforcement for ductile Engineered Cementitious Composites (ECC). *Composites Part B: Engineering*, *184*, 107741.

[8] McMullen, K. F., & Zaghi, A. E. (2021). Rapid rehabilitation of deteriorated beam ends with ultra-high performance concrete. In *Bridge Maintenance, Safety, Management, Life-Cycle Sustainability and Innovations* (pp. 1706-1713). CRC Press.

[9] Sturm, A. B., Visintin, P., & Oehlers, D. J. (2020). Blending fibres to enhance the flexural properties of UHPFRC beams. *Construction and Building Materials*, *244*, 118328.

[10] Donnini, J., Lancioni, G., Chiappini, G., & Corinaldesi, V. (2021). Uniaxial tensile behavior of ultra-high performance fiber-reinforced concrete (uhpfrc): Experiments and modeling. *Composite Structures*, *258*, 113433.

[11] Tran, N. T., Nguyen, D. L., Kim, D. J., & Ngo, T. T. (2021). Sensitivity of various fibre features on shear capacities of ultra-high-performance fibre-reinforced concrete. *Magazine of Concrete Research*, 1-17.

[12] Tam, C. M., Tam, V. W., & Ng, K. M. (2012). Assessing drying shrinkage and water permeability of reactive powder concrete produced in Hong Kong. *Construction and Building Materials*, *26*(1), 79-89.

[13] Dong, Y. (2018). Performance assessment and design of ultra-high performance concrete (UHPC) structures incorporating life-cycle cost and environmental impacts. *Construction and Building Materials*, *167*, 414-425.

[14] Yu, R., Spiesz, P., & Brouwers, H. J. H. (2014). Mix design and properties assessment of ultra-high performance fibre reinforced concrete (UHPFRC). *Cement and concrete research*, *56*, 29-39.

[15] Wille, K., El-Tawil, S., & Naaman, A. E. (2014). Properties of strain hardening ultra high performance fiber reinforced concrete (UHP-FRC) under direct tensile

loading. *Cement and Concrete Composites*, *48*, 53-66.

[16] Naaman, A. E. (2003). Engineered steel fibers with optimal properties for reinforcement of cement composites. *Journal of advanced concrete technology*, *1*(3), 241-252.

[17] Maalej, M., & Li, V. C. (1994). Flexural/tensile-strength ratio in engineered cementitious composites. *Journal of Materials in Civil Engineering*, *6*(4), 513-528.

[18] Joo Kim, D., El-Tawil, S., & Naaman, A. E. (2009). Rate-dependent tensile behavior of high performance fiber reinforced cementitious composites. *Materials and Structures*, *42*(3), 399-414.

[19] Tran, T. K., & Kim, D. J. (2013). Investigating direct tensile behavior of high performance fiber reinforced cementitious composites at high strain rates. *Cement and Concrete Research*, *50*, 62-73.

[20] Kanakubo, T. (2006). Tensile characteristics evaluation method for ductile fiber-reinforced cementitious composites. *Journal of Advanced Concrete Technology*, *4*(1), 3-17.

[21] Naaman, A. E., & Homrich, J. R. (1989). Tensile stress-strain properties of SIFCON. *Materials Journal*, *86*(3), 244-251.

[22] Hassan, M. M., Schiermeister, L., & Staiger, M. P. (2015). Sustainable production of carbon fiber: Effect of cross-linking in wool fiber on carbon yields and morphologies of derived carbon fiber. *ACS Sustainable Chemistry & Engineering*, *3*(11), 2660-2668.

[23] ELG Carbon Fibre Ltd. LCA benefits of rCF (2017). In: Composite recycling & LCA; Stuttgart, Germany.

[24] Dai, Q., Kelly, J. C., Burnham, A., & Elgowainy, A. (2015). *Updated Life-Cycle Assessment of Aluminum Production and Semi-Fabrication for the GREET Model* (No. ANL/ESD-15/12). Argonne National Lab.(ANL), Argonne, IL (United States).

[25] Greene J. Sustainable plastics with reduced carbon footprint & reduced waste (2010). White Paper; Available from: http://www.sustainablegreenproducts.

[26] Yu, J., Yao, J., Lin, X., Li, H., Lam, J. Y., Leung, C. K., Sham IML, and Shih, K. (2018). Tensile performance of sustainable Strain-Hardening Cementitious Composites with hybrid PVA and recycled PET fibers. *Cement and Concrete Research*, *107*, 110-123.

[27] Keoleian, G. A., Kendall, A., Dettling, J. E., Smith, V. M., Chandler, R. F., Lepech, M. D., & Li, V. C. (2005). Life cycle modeling of concrete bridge design: Comparison of engineered cement.

[28] Kim, S. W., Jang, S. J., Kang, D. H., Ahn, K. L., & Yun, H. D. (2015). Mechanical properties and eco-efficiency of steel fiber reinforced alkali-activated slag concrete. *Materials*, *8*(11), 7309-7321.

[29] Yacout, D. M., Abd El-Kawi, M. A., & Hassouna, M. S. (2016). Cradle to gate environmental impact assessment of acrylic fiber manufacturing. *The International Journal of Life Cycle Assessment*, *21*(3), 326-336.

[30] Barber, A., & Pellow, G. (2006). LCA: New Zealand merino wool total energy use. In *5th Australian Life Cycle Assessment Society (ALCAS) conference, Melbourne* (pp. 22-24).

[31] De Fazio, P. (2011). Basalt fiber: from earth an ancient material for innovative and modern application. *Energia, Ambiente e Innovazione*, *3*, 89-96.

[32] Inman, M., Thorhallsson, E. R., & Azrague, K. (2017). A mechanical and environmental assessment and comparison of basalt fibre reinforced polymer (BFRP) rebar and steel rebar in concrete beams. *Energy Procedia*, *111*, 31-40.

[33] Song, Y. S., Youn, J. R., & Gutowski, T. G. (2009). Life cycle energy analysis of fiber-reinforced composites. *Composites Part A: Applied Science and Manufacturing*, *40*(8), 1257-1265.

[34] Vlachopoulos, J. (2009). An assessment of energy savings derived from mechanical

recycling of polyethylene versus new feedstock. *Hamilton, ON, Canada: The World Bank.*

[35] Yu, J., Yao, J., Lin, X., Li, H., Lam, J. Y., Leung, C. K., Sham IML, and Shih, K. (2018). Tensile performance of sustainable Strain-Hardening Cementitious Composites with hybrid PVA and recycled PET fibers. *Cement and Concrete Research*, *107*, 110-123.

[36] Boustead, I. (1999). Ecoprofiles of plastics and related intermediates. *Association of Plastics Manufacturers in Europe, Brussels, Belgium.*

[37] Yoo, D. Y., Kim, M. J., Kim, S. W., & Park, J. J. (2017). Development of cost effective ultra-high-performance fiber-reinforced concrete using single and hybrid steel fibers. *Construction and Building Materials*, *150*, 383-394.

[38] Meng, W., Valipour, M., & Khayat, K. H. (2017). Optimization and performance of cost-effective ultra-high performance concrete. *Materials and structures*, *50*(1), 1-16.

[39] JCI SF4, (1983). Standard Test Method for Flexural Strength and Flexural Toughness of Fiber Reinforced Concrete.

[40] NBN, B., (1992). B 15-238: Test on fibre reinforced concrete bending test on prismatic simples. *Norme Belge, Institut Belge de Normalisation. Brussels*.

[41] Teutsch, M., 2004. German guidelines on steel fiber concrete. *In Proceeding of the North American/European Workshop on Advances in Fiber Reinforced Concrete* (pp. 23-28).

[42] ASTM C1399 / C1399M, (2015). Standard Test Method for Obtaining Average Residual-Strength of Fiber-Reinforced Concrete, ASTM International, West Conshohocken, PA, www.astm.org.

[43] RILEM TC 162-TDF, (2003), "Final Recommendation of RILEM TC 162-TDF: Test and Design Methods for Steel Fibre Reinforced Concrete: σ-ε

Design Method," *Materials and Structures*, V. 36, No. 262, Oct., pp.560-567.

[44] DIN EN 14561, (2006). Chemical Disinfectants and Antiseptics – Quantitative Carrier Test for the Evaluation of Bactericidal Activity for Instruments Used in the Medical Area – Test Method and Requirements (Phase 2, Step 2).

[45] ASTM C1609 / C1609M (2019a), Standard Test Method for Flexural Performance of Fiber-Reinforced Concrete (Using Beam With Third-Point Loading), ASTM International, West Conshohocken, PA, www.astm.org.

[46] ASTM C293 / C293M, (2016). Standard Test Method for Flexural Strength of Concrete (Using Simple Beam with Center-Point Loading), ASTM International, West Conshohocken, PA, www.astm.org.

[47] Navalurkar, R.K., Hsu, C.T.T., Kim, S.K. and Wecharatana, M., (1999). True fracture energy of concrete. *Materials Journal*, *96*(2), pp.213-225.

[48] Chiaia, B., Fantilli, A.P. and Vallini, P., (2007). Evaluation of minimum reinforcement ratio in FRC members and application to tunnel linings. *Materials and Structures*, *40*(6), pp.593-604.

[49] Zhang, T.G., Leng, Y.B. and Gao, D.Y., (2010). Test for crack opening displacement of steel fiber reinforced concrete under Three-Point Bending. In *Applied Mechanics and Materials* (Vol. 36, pp. 157-161). Trans Tech Publications.

[50] Ding, Y., (2011). Investigations into the relationship between deflection and crack mouth opening displacement of SFRC beam. *Construction and Building Materials*, *25*(5), pp.2432-2440.

[51] Aslani, F. and Bastami, M., (2015). Relationship between deflection and crack mouth opening displacement of self-compacting concrete

beams with and without fibers. *Mechanics of Advanced Materials and Structures*, *22*(11), pp.956-967.

[52] Meng, W., & Khayat, K. H. (2018). Effect of hybrid fibers on fresh properties, mechanical properties, and autogenous shrinkage of cost-effective UHPC. *Journal of Materials in Civil Engineering*, *30*(4), 04018030.

[53] Eide, M. B., & Hisdal, J. M. (2012). Ultra High Performance Fibre Reinforced Concrete (UHPFRC)–State of the art: FA 2 Competitive constructions: SP 2.2 Ductile high strength concrete.

[54] ASTM C150 / C150M (2020), Standard Specification for Portland Cement, ASTM International, West Conshohocken, PA, www.astm.org.

[55] ASTM C494 / C494M (2019), Standard Specification for Chemical Admixtures for Concrete, ASTM International, West Conshohocken, PA, www.astm.org.

[56] Hegger, J., & Rauscher, S. (2008). UHPC in composite construction. In *Ultra High Performance Concrete (UHPC). Second International Symposium on Ultra High Performance Concrete. Kassel* (Vol. 5, No. 07).

[57] ASTM C39 / C39M (2021), Standard Test Method for Compressive Strength of Cylindrical Concrete Specimens, ASTM International, West Conshohocken, PA, www.astm.org.

[58] Pourbaba, M., & Joghataie, A. (2019). Determining shear capacity of ultra-high performance concrete beams by experiments and comparison with codes. *Scientia Iranica,* 26(1), 273-282.

[59] Pourbaba, M., Sadaghian, H., & Mirmiran, A. (2019). Flexural response of UHPFRC beams reinforced with steel rebars. *Adv. Civ. Eng. Mater*, 8(3), 20190129.

[60] Ahangarnazha, B. H., Pourbaba, M., & Afkar, A. (2020). Bond behavior between steel and Glass Fiber Reinforced Polymer (GFRP) bars and ultra-high performance concrete reinforced by Multi-Walled Carbon Nanotube (MWCNT). *Steel and*

Composite Structures, An International Journal, 35(4), 463-474.

[61] ATENA (2016), Finite Element Software, ATENA Program Documentation, Theory and FRC User Manual, Cervenka Consulting, Prague, Czech Republic.

[62] Farzam, M., Sadaghian, H., & Khodadade, G. (2019). Shear behaviour of elongated rectangular wall–footing connections under eccentric loads. *Magazine of Concrete Research*, *71*(1), 43-54.

[63] Farzam, M., & Sadaghian, H. (2018). Mechanical model for punching shear capacity of rectangular slab-column connections. *Structural Concrete*, *19*(6), 1983-1991.

[64] Sadaghian, H., & Farzam, M. (2019). Numerical investigation on punching shear of RC slabs exposed to fire. *Computers and Concrete*, *23*(3), 217-233.

[65] Dadmand, B., Pourbaba, M., Sadaghian, H., & Mirmiran, A. (2020a). Effectiveness of steel fibers in ultra-high-performance fiber-reinforced concrete construction. *Advances in concrete construction*, *10*(3), 195-209.

[66] Dadmand, B., Pourbaba, M., Sadaghian, H., & Mirmiran, A. (2020b). Experimental & numerical investigation of mechanical properties in steel fiber-reinforced UHPC. *Computers and Concrete*, *26*(5), 451-465.

[67] Sadaghian, H., Pourbaba, M., Andabili, S. Z., & Mirmiran, A. (2021). Experimental and numerical study of flexural properties in UHPFRC beams with and without an initial notch. *Construction and Building Materials*, *268*, 121196.

[68] Dadmand, B., Pourbaba, M., & Riahi, R. (2022). Experimental and Numerical Investigation of Different Types of Jacketing Effect on Retrofitting RC Short Columns Using ECC Concrete. *Periodica Polytechnica Civil Engineering, 66(2), 603-613.*

[69] Naderpour, H., Nagai, K., Fakharian, P., & Haji, M. (2019). Innovative models for prediction of compressive strength of FRP-confined circular reinforced concrete

columns using soft computing methods. *Composite Structures*, 215, 69-84.

[70] Suksawang, N., Wtaife, S., & Alsabbagh, A. (2018). Evaluation of Elastic Modulus of Fiber-Reinforced Concrete. *ACI Materials Journal*, *115*(2).

[71] BS EN 14651, (2007). Test method for metallic fibre concrete—Measuring the flexural tensile strength (limit of proportionality (LOP), residual). European Committee for Standardization, B-1050 Brussels.

[72] Almusallam, T., Ibrahim, S.M., Al-Salloum, Y., Abadel, A. and Abbas, H., (2016). Analytical and experimental investigations on the fracture behavior of hybrid fiber reinforced concrete. *Cement and Concrete Composites, 74*, pp.201-217.

[73] Weibull, W. (1951). A statistical distribution function of wide applicability. *Journal of applied mechanics*, *18*(3), 293-297.

[74] Bazant, Z. P., & Chen, E. P. (1997). Scaling of structural failure.

[75] Carpinteri, A., & Chiaia, B. (1997). Multifractal scaling laws in the breaking behaviour of disordered materials. *Chaos, Solitons & Fractals, 8*(2), 135-150.

[76] Kim, J. K., & Yi, S. T. (2002). Application of size effect to compressive strength of concrete members. Sadhana, 27(4), 467.

[77] Guo, Z. H. (1997). Strength and deformation of concrete. *Beijing: Tsinghua University Press*, *156*, 156.

[78] Yan, G. "Study on failure criterion and constitutive relationship of 200 MPa reactive powder concrete (RPC200)." *Beijing Jiaotong University Doctoral Dissertation* (2005).

[79] Wang, L. M., & Xu, S. L. (2002). Characteristic curve of concrete and fiber reinforced concrete. *Journal-Dalian University of Technology*, *42*(5), 580-585.

[80] Wu, Z., Shi, C., He, W., & Wu, L. (2016). Effects of steel fiber content and shape on mechanical properties of ultra-high performance concrete. *Construction and building materials*, *103*, 8-14.

[81] Dehnavipour, H., Mehrabani, M., Fakhriyat, A., & Jakubczyk-Gałczyńska, A. (2019). Optimization-based design of 3D reinforced concrete structures. *Journal of Soft Computing in Civil Engineering*, *3*(3), 95-106.

[82] Nagaraj, A. (2021). Rheology of Fresh Concrete-A Review. *Journal of Rehabilitation in Civil Engineering*.

[83] Naderpour, H., Rafiean, A. H., & Fakharian, P. (2018). Compressive strength prediction of environmentally friendly concrete using artificial neural networks. *Journal of Building Engineering, 16, 213-219.*

[84] Skazlić, M., & Bjegović, D. (2009). Toughness testing of ultra-high performance fibre reinforced concrete. *Materials and Structures*, *42*(8), 1025-1038.

[85] Walraven, J. C. (2009). High performance fiber reinforced concrete: progress in knowledge and design codes. *Materials and Structures, 42(9), 1247-1260.*